Loss of CD36 protects against diet-induced obesity but results in impaired muscle stem cell function, delayed muscle regeneration and hepatic steatosis

Article

Accepted Version

Research article

Title

Loss of CD36 protects against diet-induced obesity but results in impaired muscle stem cell function, delayed muscle regeneration and hepatic steatosis

Sandrine Verpoorten[1], Peggy Sfyri[1], David Scully[1], Robert Mitchell[2], Anastasia Tzimou[3], Vassilis Mougios[3], Ketan Patel[2], Antonios Matsakas[1]

[1]Molecular Physiology Laboratory, Centre for Atherothrombosis & Metabolic Disease, Hull York Medical School, University of Hull; [2]School of Biological Sciences, University of Reading; [3]Laboratory of Evaluation of Human Biological Performance, School of Physical Education and Sports Science at Thessaloniki, Aristotle University of Thessaloniki

Short title: Loss of CD36 affects muscle stem cells in DIO

Address correspondence to
Dr. Antonios Matsakas
Molecular Physiology Laboratory
Centre for Atherothrombosis & Metabolic Disease
Hull York Medical School
University of Hull
Cottingham Road
Hull, HU6 7RX
United Kingdom
Tel: +44(0)1482465008
Email: Antonios.Matsakas@hyms.ac.uk

Abstract

Aim: The prevalence of obesity is a major risk factor for cardiovascular and metabolic diseases including impaired skeletal muscle regeneration. Since skeletal muscle regenerative capacity is regulated by satellite cells, we aimed to investigate whether a high-fat diet impairs satellite cell function and whether this is linked to fatty acid uptake via CD36. We also aimed to determine whether loss of CD36 impacts on muscle redox homeostasis and skeletal muscle regenerative capacity.

Methods: We studied the impact of a high-fat diet and CD36 deficiency on murine skeletal muscle morphology, redox homeostasis, satellite cell function, bioenergetics and lipid accumulation in the liver. We also determined the effect of CD36 deficiency on skeletal muscle regeneration.

Results: High-fat diet increased body weight, intramuscular lipid accumulation and oxidative stress in wild-type mice that were significantly mitigated in CD36-deficient mice. High-fat diet and CD36 deficiency independently attenuated satellite cell function on single fibres and myogenic capacity on primary satellite cells. CD36-deficiency resulted in delayed skeletal muscle regeneration following acute injury with cardiotoxin. CD36-deficient and wild-type primary satellite cells had distinct bioenergetic profiles in response to palmitate. High-fat diet induced hepatic steatosis in both genotypes that was more pronounced in the CD36 deficient mice.

Conclusion: This study demonstrates that CD36 deficiency protects against diet-induced obesity, intramuscular lipid deposition and oxidative stress but results in impaired muscle satellite cell function, delayed muscle regeneration and hepatic steatosis. CD36 is a key mediator of fatty acid uptake in skeletal muscle, linking obesity with satellite cell function and muscle regeneration.

Key words: high-fat diet, obesity, CD36 deficiency, satellite cells, oxidative stress, regeneration

Introduction

Skeletal muscle stem cells, also called satellite cells, are the major source of newly forming myoblasts and of crucial importance for postnatal muscle growth, maintenance, regeneration and hypertrophy [1 2 3]. Satellite cells are located between the basal lamina and the sarcolemma, where they reside in a mitotically quiescent state in the healthy adult skeletal muscle [1,4]. Upon stimulation by muscle maintenance pathways or injury, satellite cells exit their quiescent state and enter the cell cycle. The vast majority will then continue to proliferate and differentiate towards the myogenic lineage, forming new myoblasts, whereas a small number of satellite cells return to a quiescent state, replenishing the skeletal muscle stem cell pool [1 2 3]. Satellite cell function is a complex and tightly regulated process with particular relevance for muscle biology and metabolism. Impaired satellite cell function has been associated with a variety of muscle diseases such as Duchenne muscular dystrophy and age-related sarcopenia [5,6].

Additionally, accumulating evidence shows that skeletal muscle function and regeneration is compromised in obesity and type 2 diabetes [7-12]. Perturbed muscle metabolic capacity leads to insulin resistance, increased fatty acid uptake and intramuscular triacylglycerol accumulation in skeletal muscle of obese and diabetic individuals [13-16]. CD36, as one of the major fatty acid transporters in skeletal muscle [17], has been shown to be upregulated under high-fat diet conditions [18,19] further facilitating the transport and ectopic accumulation of lipids. Translocation and elevated expression of CD36 in various tissues such as cardiac tissue [20-22] and skeletal muscle [23] result in lipid overload and lipotoxicity [24] accelerating the development of metabolic disorders, collectively described as the metabolic syndrome. Although previous studies have already revealed several unfavourable changes in the obese condition,

such as increased susceptibility to muscle damage [25,26], decline in general muscle health and impaired regenerative capacity [10,27], the underlying cellular and metabolic changes are still poorly understood.

Given the importance of the skeletal muscle function and metabolism in the context of obesity and diabetes, it is paramount to understand the mechanism linking obesity and impaired muscle health. Since skeletal muscle regenerative capacity is regulated by the satellite cell function, we aimed to investigate the effects of diet-induced obesity on satellite cell function. We hypothesised that obese mice would display impaired satellite cell function due to lipid overload of skeletal muscle tissue. Specifically, we sought to examine whether high-fat diet (HF) impaired satellite cell function that can be linked to fatty acid uptake *via* CD36. Furthermore, we aimed to determine whether loss of CD36 impacts on muscle redox homeostasis and skeletal muscle regenerative capacity.

Results

CD36 knockout mice are protected from weight gain in response to high-fat diet. To determine whether loss of CD36 protects from weight gain, wild-type (WT) and CD36 knockout (KO) mice were fed a HF diet (HF) or a normal diet (ND) for 13 weeks (**Figure 1A**). Body weight was recorded weekly, including the final body weight at week 13 (**Figure 1B-D**). HF diet gradually increased body weight in WT mice starting from week 4 which was more pronounced by week 13, compared to mice fed a ND (**Figure 1C, D**). WT mice displayed an increased bodyweight by 37% after 13 weeks of HF diet and developed obesity compared to the WT littermates maintained on a standard laboratory chow (ND). Conversely, CD36 KO mice fed a HF diet showed decreased body weight gain compared to the WT HF group (i.e. 14 versus 37% respectively; interaction p=0.009) and no significant difference when compared to WT ND (1%) or CD36 KO ND (14%) mice (**Figure 1C, D**). We further found the weights of the soleus (Sol) and biceps brachii (BB) muscles to be increased by HF diet in the WT, but not the KO animals. Most strikingly, we found the white adipose tissue (WAT) weight to be significantly higher in WT HF diet animals (2-fold; significant interaction p=0.0012) when compared to HF diet CD36 KO mice (**Supplementary Figure 1A-F**). These findings indicate that CD36-deficient mice are protected from HF diet-induced obesity.

CD36 KO mice show reduced lipid accumulation in skeletal muscle in response to high-fat diet. Intramuscular assessment of neutral lipid content was measured by BODIPY staining. The HF diet induced significantly higher lipid accumulation in the tibialis anterior (TA) muscle in WT mice (p<0.001; **Figure 2A, B**). In contrast, HF diet failed to induce a significant increase in BODIPY staining in CD36 KO mice. These findings were confirmed by quantifying intramuscular triacylglycerol (TG) accumulation

by gas chromatography. Total phospholipid content was significantly lower in CD36 KO mice independent of diet (**Figure 2C**). Given that HF diet is often associated with morphological changes of the skeletal muscle [28], we investigated muscle specific changes of fibre type composition and size. Immunohistochemistry revealed a significant reduction in number and size of type IIB fibres of the extensor digitorum longus (EDL) muscle in WT HF versus WT ND. No significant changes were found in soleus with regard to genotype or diet (**Supplementary Figure 2**). We next examined the expression of genes involved in fatty acid uptake and utilization as well as cross-talk between adipose tissue and skeletal muscle using quantitative reverse-transcription polymerase chain reaction (qRT-PCR). Relative mRNA expression of Fibronectin type III domain-containing protein 5 (*Fndc5*) and Interleukin 15 (*IL-15*) revealed a significant increase in CD36 KO HF diet mice compared to WT ND and HF mice. Furthermore, mRNA levels of Fatty acid binding protein 3 (*Fabp3*) and Carnitine palmitoyltransferase I (*Cpt1*) were significantly increased in CD36 KO mice (*Cpt1*) or both in WT and CD36 KO mice on a HF diet (*Fabp3*) when compared to control littermates **(Figure 2D)**.

Skeletal muscle from CD36 KO mice is protected from high-fat diet-induced oxidative stress. Recent evidence indicates a direct link between the production of diet-induced reactive oxygen species (ROS) and levels of oxidative protein modifications such as 4-hydroxynonenal (4-HNE) and 3-nitrotyrosine (3NT) adducts that are involved in the development of metabolic disorders [29-32]. Loss of CD36 is known to attenuate ROS production, alleviating oxidative stress [33,34]. Therefore, we sought to determine the impact of CD36 deficiency and HF diet on the redox homeostasis of the skeletal muscle, by measuring lipid peroxidation (thiobarbituric acid reactive substance; TBARS), protein oxidative modifications (3NT, 4-HNE), DNA

damage (by means of *Ogg1* relative mRNA expression) and ROS production (Dihydroethidium; DHE staining).

Skeletal muscle TBARS levels were significantly increased in the WT HF diet group compared to the WT ND group which is in line with previous evidence [35]. In contrast, HF diet CD36 KO mice showed TBARS level comparable to the CD36 ND and WT ND control group (**Figure 3A**). 4-HNE protein adducts were significantly higher in WT HF mice compared to WT ND (**Figure 3B, C**). However, CD36 KO mice fed a HF diet showed no sign of elevated 4-HNE protein adducts when compared to their CD36 KO ND littermates or WT ND mice. Similarly, WT HF diet mice displayed an increase in 3NT levels (**Figure 3B, D**), which is an indirect marker of increased ROS levels, leading to increased protein oxidative modification. Moreover, CD36 KO mice under HF diet had similar 3NT levels to WT ND and CD36 KO ND groups.

We next determined the relative mRNA expression levels of 8-Oxoguanine glycosylase (*Ogg1*; DNA repair enzyme), Nicotinamide adenine dinucleotide phosphate oxidase 2 (*Nox2*; oxidative stress marker), Catalase, Peroxiredoxin-1 and microsomal Glutathione S-Transferase 1 (*Cat, Prdx1, Mgst1, Sod1*; antioxidant genes) by qRT-PCR. There were no significant changes between any of the cohorts in the relative mRNA expression level of DNA-repair gene *Ogg1*, nor the oxidative-stress marker *Nox2* (**Figure 3E**). However, the gene expression of the anti-oxidant enzyme Catalase was significantly upregulated in WT HF diet (2-fold), CD36 KO ND (1.4- fold) and CD36 KO HF diet (2.2-fold) animals when compared to WT ND (**Figure 3F**). Furthermore, we found increased mRNA levels of the antioxidant gene *Prdx1*, *Mgst1* and *Sod1* in CD36 KO on a HF diet when compared to WT ND and CD36 KO ND (**Figure 3F**).

We next aimed to investigate the impact of increased fatty acid availability on oxidative stress levels in myotubes derived from satellite cells. Following 5 days of myoblast differentiation, myotubes from WT and CD36 KO animals were treated with palmitate (PA) and stained with DHE as an indicator for ROS production. We found a significantly increased number of DHE positive (+ve) myoblast nuclei in WT cell cultures treated with palmitate, compared to WT DM and CD36 KO cells treated with PA for 24 hours. CD36 KO cultures had significantly lower DHE levels compared to WT myotubes which was confirmed *in vivo* on EDL muscle sections (**Figure 3G, H and Supplementary Figure 3**). Similarly, WT myotube cultures treated with PA had significantly increased numbers of DHE^{+ve} nuclei per myotube when compared to WT DM or CD36 KO treated with PA (**Figure 3G, H**). Moreover, the nuclear size was significantly lower in WT myotubes treated with PA but not in CD36 KO cultures treated with PA (**Figure 3H**). Shrinking nuclear size has been previously correlated with hypoxia-induced cell death [36]. Taken together, these data suggest that ectopic fat accumulation in skeletal muscle of WT mice is primarily linked to increased oxidative stress, while skeletal muscle of CD36 KO mice is protected from oxidative stress, partly due to increased antioxidant enzyme activity.

CD36 KO satellite cells maintain their proliferative capacity but have compromised differentiation after a high-fat diet. Given that lipid accumulation in the skeletal muscle is primarily involved in increased oxidative stress, we next aimed to examine the impact of HF diet on the satellite cell function on cultured mature muscle fibres stained for Pax7, MyoD and Myogenin. We found that the total satellite cell number and the ratio of myonuclei per satellite cell were similar at baseline among the experimental groups independent of diet or genotype (0 hours). However, the total number of satellite cells was significantly lower in the WT HF diet group compared to

WT ND, CD36 KO ND and CD36 KO HF diet animals after 24 and 48 hours of culture (**Figure 4A-D**). Whilst both CD36 KO ND and CD36 KO HF diet groups showed no sign of decreased total satellite cell number up to 48 hours of culture, we found a significant decrease in satellite cell number at 72 hours of culture in all groups compared to WT ND (**Figure 4C**). These results suggest that long-term HF diet feeding has a negative impact on satellite cell proliferation and commitment to differentiation, which is linked to fatty acid uptake *via* CD36. Taken together, CD36 appears to play a key role during myocyte terminal differentiation, indicated by the diet-independent decrease in satellite cell number at 72 hours in the CD36 KO animals.

Isolated satellite cells from CD36 KO mice have impaired myogenic capacity. Given the impaired satellite cell function on single fibres after 72 hours cell-culture in response to HF diet and CD36 deficiency, we next studied the function of CD36 in isolated satellite cells from the EDL and BB muscles *in vitro* (**Figure 5A**). We observed severely compromised satellite cell differentiation and myotube formation in the CD36 deficient culture after 5 days of induced differentiation, evidenced by a significantly lower Myogenin/DAPI (%) ratio (Total of DAPI stained nuclei divided by all myogenin^{+ve} nuclei) as well as a significantly lower fusion index (FI; Myogenin^{+ve} nuclei inside mature myotubes divided by total DAPI) (**Figure 5B**). Not only do these results suggest a severely impaired differentiation of satellite cells derived from CD36 deficient mice, but also indicate a deficit in myotube formation. These findings were obtained in independent experiments of satellite cells from both the EDL and BB muscle.

We next examined the expression profile of genes involved in the maturation and fusion of satellite cells during the early (i.e. 1 day in differentiation medium) and late

differentiation (i.e. 5 days in differentiation medium) by qRT-PCR and MAPKs phosphorylation by a proteome profiler array. Relative mRNA expression of Myogenin, myoblast fusion factor/myomaker (*Tmem8c*), skeletal muscle alpha-actin (*Acta1*), Myosin heavy chain type I (*Mhc1*), Serum response factor (*Srf*), and Brain expressed x-linked gene 1 (*Bex1*) revealed a significant decrease in the mRNA levels of *Srf* and *Bex1* during late differentiation of satellite cells isolated from CD36 deficient mice **(Figure 5C)**. Impaired myogenic differentiation of CD36 KO isolated satellite cells was also confirmed by impaired protein levels of Desmin, SRF and BEX1 (**Supplementary Figure 4**). In addition, MAPKs phosphorylation levels were overall decreased in CD36 KO HF muscle lysates with the exception of p38α$^{T180/Y182}$ which was 6-fold higher than CD36 KO ND (**Supplementary Figure 5**). These results suggest that CD36 plays a crucial role during satellite cell terminal differentiation and maturation with possible implications for skeletal muscle regeneration.

Palmitate treatment and CD36 deficiency independently compromise the differentiation capacity of isolated satellite cells in culture. To further study the effects of CD36 and/or increased fatty-acid availability on muscle stem cell differentiation, we treated isolated satellite cells from WT animals with the potent and irreversible CD36 inhibitor Sulfo-N-succinimidyl oleate (SSO). Once confluent the cells were further treated with palmitate (PA) to mimic the HF diet condition in a cell culture setting. Co-immunostaining of Myogenin and DAPI was used to identify differentiated satellite cells (**Figure 6A**). After 5 days of culture in differentiation medium, we found a significant decrease in the number Myogenin positive nuclei in satellite cells isolated from WT mice when treated with PA or SSO+PA and CD36 KO +/-PA, compared to WT (**Figure 6B**). Furthermore, we assessed the fusion index (FI), calculated by the number of Myogenin^{+ve} nuclei inside mature myotubes divided by total DAPI. We found

a significantly lower fusion index in satellite cells from WT+PA, CD36KO, CD36 KO+PA as well as in WT+SSO +PA groups, indicating that both PA treatment and/or CD36 deficiency lead to impaired myoblast fusion (**Figure 6C**). These data further support our previous findings, suggesting that both CD36 deficiency and increased fatty acid availability negatively impact satellite cell differentiation.

Oxidative stress has been reported to impact on muscle stem cell activity and myogenic potential [37]. We therefore studied muscle stem cell differentiation under palmitate treatment in response to two substances with known antioxidant properties (i.e. Ebselen and TEMPOL [38]. We found that palmitate increased DHE and decreased MHC levels in WT but not CD36 KO cultures of isolated satellite cells which were reversed by the use of Ebselen and TEMPOL (**Supplementary Figures 6).** The findings were also confirmed through DHE and myogenin staining in single fibre cultures (**Supplementary Figures 7).** These data indicate that treatment with antioxidant substances do not rescue CD36 KO myoblast differentiation in response to palmitate but are important for the WT cohorts.

Isolated CD36 KO and WT satellite cells have distinct bioenergetic profiles in response to palmitate treatment. Recent reports demonstrated that mitochondrial activity is associated with specific lineage decision [39]. We wished to determine if CD36 deficiency alters mitochondrial function in undifferentiated and mature, differentiated satellite cells. Further we aimed to investigate the bioenergetic profile in the presence or absence of high free fatty acid availability. To investigate this, we cultured isolated satellite cells from WT and CD36 KO mice in a Seahorse extracellular flux culture plate and used the oxygen consumption rate (OCR) to measure mitochondrial respiration in satellite cells (**Figure 7A**). Undifferentiated primary myoblasts (i.e. 1 day after isolation) revealed no significant difference in the basal OCR or coupling efficiency

(i.e. Basal OCR minus OCR after Oligomycin injection; Proton leak) (**Figure 7B, C**). Although the maximum respiratory capacity showed no difference between WT and CD36 deficient cells, the spare respiratory capacity (SRC) in CD36 deficient cells was significantly higher than in the WT cells, indicating that mitochondrial bioenergetics are altered and CD36 deficient cells are more resistant to stress, further supporting the concept that the CD36 deficient cells have an increased ability to adapt to stressful conditions. We found no difference in the non-mitochondrial respiration (Non-mit. Resp.), but a significant reduction in ATP production in the CD36 KO-derived satellite cells compared to WT-derived satellite cells (**Figure 7B, C**). We further aimed to establish the effect CD36 on mitochondrial function during satellite cell differentiation in the presence or absence of palmitate. We therefore cultured satellite cells in a seahorse extracellular flux cell culture plate until confluent and subsequently changed to differentiation medium (DM). Following differentiation (5 days DM) WT myotubes showed a significant increased basal respiration when treated with palmitate, whilst CD36 deficient myotubes revealed a reduction in the basal OCR compared to WT untreated mitochondria. The addition of the ATP synthase inhibitor Oligomycin (complex V inhibitor) decreased the OCR following injection, revealing an increased Proton leak (i.e. Basal OCR minus OCR after Oligomycin injection) in WT derived satellite cell mitochondria when treated with palmitate. Subsequently FCCP, an uncoupling agent, was injected to measure maximal oxygen consumption (i.e. complex IV). The addition of FCCP showed comparable maximal respiration (Max. Resp.) as well as unaltered spare respiratory capacity in all groups (**Figure 7D, E**). Interestingly, palmitate treatment had adverse effects on WT and CD36 deficient myotubes, increasing the spare respiratory capacity (SRC) in WT but decreasing SRC in CD36 deficient myotubes, depicted by the steep rise of OCR in the WT+PA group,

peaking shortly after the FCCP injection. Interestingly, the addition of FCCP did not lead to a further increase of the OCR in the CD36 KO+PA condition when compared to CD36 KO OCR (**Figure 7E**). We found ATP production to be elevated only in the WT+PA condition (**Figure 7D, E**). In all, our data suggests that myotube mitochondria have an altered bioenergetic response in the presence of palmitate which seems to be, at least partly, regulated through CD36.

CD36-deficiency results in delayed skeletal muscle regeneration following acute injury with cardiotoxin. Having shown that CD36 KO derived satellite cells exhibit reduced commitment to differentiation, we next examined the impact of CD36 deficiency on skeletal muscle regeneration *in vivo*. Regeneration of skeletal muscle is mainly driven by a highly orchestrated process involving the activation, proliferation, differentiation and fusion of satellite cells [40]. Following cardiotoxin (CTX) injection in the tibialis anterior, necrotic tissue and damaged fibres are replaced by newly formed fibres expressing embryonic myosin heavy chain (eMHC). Here we show that the cross-sectional area (CSA) of early regenerating fibres expressing ($eMHC^{+ve}$ at day 5) was comparable between WT and CD36 KO mice (**Figure 8A**). However, the clearance of necrotic fibres (by means of IgG infiltration) was significantly impaired in CD36 KO mice when compared to WT animals at 5 days after the CTX injury. Along with this finding we show a significant decrease in macrophage infiltration and muscle progenitor cell density expressing Myogenin (but not MyoD) in CD36 KO mice 5 days after CTX injury (**Figure 8A and Supplementary Figure 8**). Furthermore, we found significantly smaller CSA of regenerating fibres 10 days after CTX injection (**Figure 8B, D**) in CD36 KO mice. In line with this observation, we report that regenerating fibres expressing eMHC were absent in WT but still present in CD36 KO mice 10 days after CTX injury. Taken together, these data suggest delayed skeletal muscle

regeneration in CD36 KO mice based on higher frequency of necrotic fibres, reduced CSA of regenerating fibres and decreased macrophage infiltration.

CD36 KO mice develop hepatic steatosis in response to high-fat diet. Additionally, we aimed to determine the impact of CD36 deficiency on the liver of the CD36 KO mouse. WT mice on a HF diet showed a significant increase in lipid accumulation in the liver as shown by Oil red O staining compared to WT and CD36 KO mice on a standard chow. Remarkably, CD36 KO mice exhibited a significant increase of lipid accumulation compared to all other groups, as evidenced by the larger lipid number as well as lipid size (**Figure 9A-B**). These findings were supported by quantifying hepatic TG accumulation using gas chromatography. However, total phospholipid content was not affected by either genotype or diet (**Figure 9C**). These results prompted us investigate expression profiles of genes involved in fatty acid transport and metabolism in the liver. Levels of relative mRNA expression of Fatty acid transporter proteins 1,2,3 and 5 (*Fatp1,2,3,5*) and *Pparγ* as well as cell death-inducing DNA fragmentation factor α-like effector A (*Cidea)* were quantified. *Fatp2*, *Fatp1* and *Pparγ* were significantly increased in CD36 KO HF diet animals when compared to WT ND mice. Most strikingly, we found that expression of *Cidea*, which has been shown to regulate lipolysis and lipid fusion [41,42], was increased 25-fold in CD36 KO mice compared to control mice (**Figure 9D**). Collectively, this data indicates opposing effects of CD36 deficiency with a protective role in the skeletal muscle due to reduced lipid accumulation, but at the same time leading to excessive lipid deposition in the liver.

Material and methods

Mice. All experiments were in accordance with UK Animals Scientific Procedures Act 1986. This study was carried out on male Wild-type (WT; C57/Bl6) and CD36 knockout (KO) mice. Whole-body CD36 KO mice were previously created via targeted homologous recombination. Exon3, which contains the first 40 amino acids of CD36, was deleted entirely in the homologous recombined allele [43]. Mice were maintained in a temperature- and humidity-controlled facility with 12/12 h light/dark cycle and had ad libitum access to water and food. At 2-3 months of age, a subset of mice was randomly distributed into a standard laboratory chow group (product "5LF5-EURodent Diet 22%", LabDiet, St.Louis, USA) and a high-fat diet (SDS 824053 High-Fat diet, 45%, SDS Diets Grangemouth, Falkirk, UK) group for a period of 13 weeks. Mice were then sacrificed using a CO_2 overdose. Muscle, adipose, heart and liver tissue were excised, weighed, snap frozen and covered in optimum cutting temperature embedding compound (OCT) and stored at -80°C until further use.

Single fibre isolation and cell culture. Single muscle fibres were obtained by precise dissection of the Extensor digitorum longus (EDL) and the Biceps Brachii (BB) muscle, followed by collagenase digestion (0.2%; Sigma Aldrich; cat. C2674) as previously described [44]. Briefly, following collagenase digestion, the muscle tissue was transferred into a horse serum (Gibco) coated petri dish and triturated using a wide-bore glass pipette to dissociate individual fibres. Floating single fibres were then cultured for 24, 48 or 72 hours in growth medium (GM; 10% horse serum, 0.5% chicken embryo extract) ± Palmitate (0.3mM) ± Ebselen (20μM; cat. E3520-100MG, Sigma, UK). Subsequently the fibres were stained for the satellite cell-specific markers Pax7 (1:200, mouse monoclonal anti-Pax7, Santa Cruz, cat. Sc81648), MyoD (1:200, rabbit polyclonal anti-MyoD, Santa Cruz, cat. sc-760) and Myogenin (1:200, rabbit

polyclonal anti-Myogenin, Santa Cruz, cat. sc-576); nuclei were counterstained using 4,6-diamidino-2-phenylindole (DAPI, Sigma Aldrich, UK). Satellite cell expression profiles from isolated single fibres (N=50 per condition) was assessed using N=5 animals per group.

Satellite cell isolation from single fibres. Primary myoblasts were derived from isolated single fibres after collagenase digestion as described above. Subsequently, the fibres were incubated in 1mL 0.125% Trypsin-EDTA for 5 minutes and centrifuged at 210 x g. Cells were suspended in 3mL Satellite cell proliferation medium (PM; 30% Foetal bovine serum, 1.5% chicken embryo extract in Dulbecco's Modified Eagles Medium, high glucose, Pyruvate supplemented) and were transferred into Matrigel-coated cell culture dishes (cat. 354234, Corning, Bedford, USA, final concentration 1mg ml^{-1}), followed by a three-day incubation. Subsequently, floating single fibre fragments were removed, medium was changed to growth medium (GM; 10% Foetal bovine serum, 0.5% chicken embryo extract in DMEM) and isolated satellite cells were cultured until they reached 80% confluence. Each preparation typically yields 2-3 $x10^5$ cells per cell culture dish (originating from approximately 800 fibres). Induced primary myoblast differentiation was achieved through changing the GM to differentiation medium (DM; 5% horse serum, 0.5% chicken embryo extract in DMEM) for 5 subsequent days. Palmitate treatment was performed using 0.3mM final concentration and Sulfo-N-succinimidyl oleate (SSO) induced CD36 inhibition at a final concentration of 0.25mM. Cellular antioxidant experiments were conducted with ± Palmitate (0.3mM) ± Ebselen (20μM) ± TEMPOL (1mM; cat. 176141-25G, Sigma, UK). Cells were fixed and differentiation confirmed visually by staining for Myogenin (1:200, rabbit polyclonal anti-Myogenin, Santa Cruz, cat. sc-52903). Nuclei were counterstained with DAPI (DAPI, Sigma Aldrich, UK). Digital images were obtained using a Zeiss AxioImager.A1,

HBO 100 fluorescent microscope. The Myogenin/DAPI ratio and the fusion index (i.e. Myogenin^{+ve} nuclei inside myotubes/total DAPIx100) were calculated using the ZEN Image software.

Immunohistochemistry. Muscle tissue (TA, EDL, Sol) was snap frozen using isopentane, cooled in liquid nitrogen and sectioned (10 µm thick). Muscle sections were permeabilised (Triton X-100 in PBS) followed by the immunofluorescent staining of two different myofibre types. Primary antibodies used were MHCIIA (DSHB A4.74) and MHCI (DSHB A4.840) or type MHCIIB (DSHB BF.F3). Incubation with primary antibodies was performed at 4°C overnight. Sections were stained with corresponding secondary antibodies (1:200) for 1 h. Images were taken using a Zeiss Axio Imager A.1 microscope (Zeiss, Germany).

BODIPY staining for muscle lipid accumulation. BODIPY staining was performed to examine lipid accumulation in TA muscle tissue after 13 weeks of HF diet or standard laboratory chow. Briefly, after cryostat-sectioning, TA tissue was incubated with 20µg/mL BODIPY solution (BODIPY®, 4,4-Difluoro-1,3,5,7,8-Pentamethyl-4-Bora-3a,4a-Diaza-s-Indacne, Fisher Scientific, UK) for 30 minutes and subsequently washed with PBS for 10 minutes. Nuclei were counterstained with DAPI (DAPI, Sigma Aldrich, UK). Digital images were obtained using a Zeiss AxioImager.A1, HBO 100 fluorescent microscope.

Western blotting. Protein was extracted from homogenised quadriceps muscle using RIPA lysis buffer 1% v/v Nonidet P40 substitute (NP-40, Sigma Aldrich, UK), 0.1% w/v SDS (Fisher Scientific, UK) and 0.5% (w/v) sodium deoxycholate (Sigma Aldrich, UK) in 50 ml PBS. Samples were centrifuged at 4°C for 15 minutes at 14,000g. Quantification of protein content from the supernatant was performed by Pierce BCA protein assay kit (Fisher Scientific, UK) according to the manufacturer's instruction. 30

micrograms of protein was resolved in 10% SDS-PAGE, and immunoblotting was performed with the corresponding antibody. The following antibodies were used: 3NT (1:500; Santa Cruz; cat. 32757), 4HNE (1:1000; R&D Systems MAB3249) β tubulin (1:1000; EMD Millipore; cat. 05-661). Immunoblotting analysis was performed by probing the membranes with each antibody or β tubulin and analysed using the Odyssey Infrared Imaging System (LI-COR Biosciences, Lincoln, NE). Band density was measured using ImageJ software. The band densities were normalized to β tubulin content.

Phospho-MAPK Proteome profiler array. MAPK phosphorylation was measured with the phosphor-MAPK proteome profiler array following the manufacturer's instructions (cat. ARY002B, R&D, UK). Pooled samples of six gastrocnemius muscles from WT ND, WT HF, CD36 KO ND and CD36 KO HF groups were lysed and adjusted to 1µg/µL. Signals were detected with chemiluminescent substrate.

Lipid peroxidation. Tissue samples were homogenised and thiobarbituric acid (TBA) reactive substance (TBARS) used to analyse lipid peroxidation with the OXItek TBARS Assay Kit (Enzo Life Science, USA) as described previously (Sfyri et al. 2018). TBARS were assessed in whole muscle samples.

Dihydroethidium (DHE) staining. Plated satellite cells were washed with PBS and subsequently incubated with 10µM of DHE (Sigma-Aldrich 7008) for 10 minutes at 37°C. The cells were then washed in PBS three times with each wash lasting 5 minutes. Finally, the cells were fixed with 4% Paraformaldehyde (PFA) for 10 minutes and mounted in fluorescent mounting medium, using DAPI to counterstain cell nuclei.

Quantitative qRT-PCR. Total RNA was isolated from both cells and tissue as described previously (Paolini et al. 2018), by using the standard TRIzol method (AMRESCO RiboZol^{TM}RNA Extraction Reagent) using the E.Z.N.A total RNA kit I

(Omega Bio-Tek, USA). Briefly, RNA was purified by DNase I treatment (Roche, Indianapolis, IN, USA). Reverse transcription of 2µg total RNA was performed using the RevertAid H MinusFirst Strand cDNA Synthesis Kit (Fisher Scientific, UK) according to the manufacturer's protocol. qRT-PCR was carried out using the Applied Biosystems SYBRGreen PCR Master Mix (Fisher Scientific; cat. 4364344) in a StepOne Plus cycler (Applied Biosystems, UK). Relative gene expression was determined using the ΔΔCT method. Values of each RNA sample were normalised to cyclophilin 1 (*Cyp1*) and hypoxanthine phosphoribosyltransferase (*Hprt)* mRNA levels. Primer sequence list is available upon request.

Seahorse XFp extracellular flux measurement. Isolated satellite cells were seeded at a density of 10,000 cells per well in 8-well XF plates pre-coated with matrigel as described previously [45]. In brief, cells were pre-incubated in growth medium (DMEM, 10% horse serum, 0.5% chicken embryo extract, 1% Penicillin/Streptomycin) for 24 hours and switched to differentiation medium (DM, 2% horse serum) for 5 subsequent days. Prior to the experiment, sensor cartridges were hydrated with XF calibrate solution (pH 7.4), as recommended by the manufacturer's instructions and incubated at 37°C in a non-CO_2 environment for 24 hours. The cell culture medium was replaced with assay medium containing 1mM sodium pyruvate and incubated for one hour in a non-CO_2 incubator. Oligomycin (1µM final concentration), carbonyl cyanide 4- (trifluoromethoxy)phenylhydrazone (FCCP; 5 µM final concentration) and Antimycin (2.5 µM final concentration) were diluted in the assay medium. The Seahorse XFp Analyzer (Seahorse Biosciences) was then used to measure the oxygen consumption rate (OCR) in real time. Baseline measurements of OCR were taken before sequential injection of oligomycin, FCCP and antimycin. Seahorse data were normalised to total protein (µg) and analysed using the Wave software from

Agilent Technologies. **Gas chromatography.** Gastrocnemius and liver lipid profiling was performed by using a combination of thin-layer chromatography and gas chromatography as previously described [32,46]. Tissue was pulverised by manual mortar and pestle grinding in liquid nitrogen. Lipids were extracted from specimens with chloroform-methanol 2:1 (v/v) in the presence of 0.005% (w/v) butylated hydroxytoluene, as an antioxidant, and fixed amounts of triheptadecanoyl glycerol (Sigma, St. Louis, MO), as triacylglycerol internal standard, and diheptadecanoyl phosphatidyl choline (Larodan, Solna, Sweden), as phospholipid internal standard. An aliquot of each lipid extract was spotted on a high-performance silica gel plate (Macherey-Nagel, Düren, Germany), which was then developed in petroleum ether - diethyl ether - acetic acid 80:20:1 (v/v/v). Lipid spots were visualised under ultraviolet light after spraying the plate with 0.2% (w/v) dichlorofluorescein in ethanol. The triacylglycerol and phospholipid spots were scraped off and transferred to screw-cap tubes. Fatty acid methyl esters (FAMEs) were produced by the addition of 1 ml of methanol - sulfuric acid 96:4 (v/v) and heating at 64°C overnight. The FAMEs were then extracted with 1 ml of hexane and were separated in an Agilent 7890A gas chromatograph (Santa Clara, CA), equipped with a 30 m-long AT-WAX capillary column (Alltech, Deerfield, IL) and flame ionization detector. The column temperature was programmed from 140° to 270°C at 40°C min^{-1} and the run was held at 270°C for 4 min. The carrier gas was helium at a flow rate of 1.6 ml min^{-1}. FAMEs were quantified in the chromatograms obtained with the aid of the Agilent ChemStation software by comparing the area under their peaks to that of methyl heptadecanoate (derived from the internal standards).

Cardiotoxin (CTX) induced muscle injury *in vivo*. Tibialis anterior (TA) muscle injury was induced as previously described [45]. Briefly, mice were injected with a total

of 30µL, 50 µmol/L *Naja pallida* CTX (Latoxan, Valence France) into the TA muscle. Mice were humanely euthanized 5- and 10-days post-injury and the TA muscles were collected for subsequent immunohistochemistry.

Oil Red O staining for liver lipid accumulation. Oil Red O staining was performed to examine lipid accumulation in liver tissue after 13 weeks of HF diet or standard laboratory chow. In short, after cryostat-sectioning, liver tissue was fixed in 4% paraformaldehyde, briefly washed and subsequently incubated with the Oil Red O solution (Fisher Scientific, UK) for 10 minutes and counterstained with haematoxylin (Sigma Aldrich, UK). Lipid deposition was confirmed visually. The area of Oil Red O staining was analysed using three fields of view for each liver taking into account lipid size and frequency.

Statistical analysis. Differences between two groups were detected by Student's *t*-test. Statistical significance in experiments comparing more than 2 groups was determined by two-way ANOVA (genotype x diet), followed by Tukey post hoc test. For the detection of differences in lipid size analysis as well as CSA, the Chi square (χ^2) test was performed. All significant differences ($p<0.05$) are given in the figures and/or figure legends. Statistical analysis was carried out using Graph Pad Prism (GraphPad Software, CA, USA) or IBM SPSS software (IBM SPSS Statistics version 24). Significant differences were considered for $p<0.05$.

Discussion

Satellite cells, the myogenic precursor stem cell population of the skeletal muscle, are of pivotal importance for skeletal muscle homeostasis and regeneration [2]. Sparse evidence suggests that skeletal muscle regeneration is severely impaired in obese individuals possibly due to increased lipid deposition and perturbed satellite cell function [7,10,27,47]. The fatty acid transporter CD36 plays an important role in skeletal muscle fatty acid transport and utilisation [22,24,48]. In this study, we show that CD36-deficient mice are protected from HF diet-induced weight gain, which is in line with previous findings [49,50], but results in impaired satellite cell function, compromised myogenic differentiation, delayed muscle regeneration after acute injury and hepatic steatosis.

Enhanced lipid storage and accumulation in adipose and skeletal muscle lead to the development of obesity and insulin resistance [51,52]. Our findings of decreased fatty acid uptake and accumulation in the CD36 KO skeletal muscle under HF diet highlight the importance of CD36 for skeletal muscle energy homeostasis. Upregulation of alternative fatty acid transporters, such as *Fabp3* in CD36 KO mice on a HF diet, was not sufficient to compensate for the defect in fatty acid uptake due to the loss of CD36. Furthermore, skeletal muscle metabolism seemed to be altered, revealing increased myokine mRNA levels such as *Fndc5* and *IL-15*, which have been shown to be increased in skeletal muscle in response to exercise and downregulated in diabetic conditions [53].

Limited data suggest that skeletal muscle ectopic lipid infiltration impairs satellite cell activation leading to a decrease of skeletal muscle regeneration potential [7,27]. We observed a significant reduction in cultured satellite cell numbers in WT HF diet mice. Moreover, we showed that obesity impairs satellite cell activation during early

proliferation (i.e. 24h). The fact that satellite cell numbers were unaffected in CD36 deficient mice further supports our hypothesis that obesity impairs satellite cell function via CD36-dependent pathways. Unexpectedly, significantly lower satellite cell numbers were observed in CD36-deficient mice during differentiation independent of diet, indicating the importance of CD36 during skeletal myogenesis [54]. This was confirmed by the deficit in myogenesis of isolated satellite cells from CD36-deficient mice *in vitro*. In line with our findings are the observed effects of palmitate on differentiation of skeletal muscle stem cells. It has been shown that palmitate inhibits differentiation through a decrease in cyclin A and cyclin D1 levels [55]. Our data also suggest that compromised myogenic differentiation in response to dietary cues and increased ROS can be rescued by antioxidant treatment in WT but not CD36 KO muscle stem cells.

MAPKs play important roles in cell differentiation, fusion and myogenesis such as Akt1, Erk1/2, GSK3α/β, JNK1, HSP27 and p38α [56-59]. Changes in phosphorylation levels of the above kinases seen in CD36 KO HF mice may, at least in part, explain the impaired myogenic differentiation reported here. Similarly, p38α levels and the p38α downstream target HSP27 were found to be hypo-phosphorylated in CD36 KO ND mice, but HSP27 phosphorylation by p38α is required for differentiation [58]. Together, these observations suggest an important role of p38α and HSP27 in the defective myogenesis of CD36 KO mice.

We further consolidated our hypothesis by quantifying gene expression of myogenic markers. We found reduced *Bex1* mRNA levels in differentiated satellite cells from CD36-deficient mice. Interestingly, *Bex1*-deficiency has been associated with prolonged proliferation and delayed differentiation following recovery after myotrauma [60]. One possible explanation for the involvement of CD36 in skeletal myogenesis is its

interaction with AMPK. CD36 has been shown to inhibit AMPK activation and in the absence of CD36, AMPK has been shown to be constitutively active in muscle [61]. This could possibly lead to the activation and proliferation of satellite cells via non-canonical Sonic Hedgehog signalling which induces Warburg-like glycolysis in satellite cells, required for their activation and proliferation during muscle regeneration [62]. AMPK also inhibits myoblast differentiation through PGC-1alpha-dependent pathways [63]. Moreover, AMPK has been shown to inhibit mTOR signalling [64], via the AMPK-Nampt-Sirt1 pathway [65], resulting in the inhibition of differentiation. This line of thought offers a plausible explanation for the adverse effect of CD36 deficiency on satellite cell proliferation and differentiation.

Mitochondrial dysfunction has been observed in several diseases related to the metabolic syndrome and is one of the most prominent abnormalities found in skeletal muscle of obese and diabetic individuals [66-68]. CD36 is involved in mitochondrial fatty acid oxidation, translocating from the cytoplasm to the mitochondrial plasma membrane during muscle contraction [69]. To assess whether loss of CD36 changes mitochondrial function in the presence of free fatty acids, we analysed the oxidative capacity and the bioenergetic profile of isolated satellite cells during proliferation and differentiation. In our study, proliferating satellite cells from CD36-deficient mice had a significantly increased spare respiratory capacity (SRC). SRC is a critical factor implicated in cell survival and function, reflecting the ability of mitochondria to maintain energy production in response to an increase in energy demand, like in acute or chronic stress [70]. These findings further support the notion that proliferating satellite cells from CD36-deficient mice have an increased ability to adapt to stressful conditions such as FCCP treatment.

We further report a decrease in ATP production in proliferating, CD36 KO derived satellite cells compared to WT-derived satellite cells. Stem cells have a low demand in ATP, which has been linked to preserved stemness [71]. A possible explanation is that, in order to produce ATP, mitochondria must utilise a substrate such as fatty acids. The reduced capacity of satellite cells from CD36 KO mice to use fatty acids for ATP production may explain the lower ATP levels during stimulated respiration [72]. Part of the myoblast differentiation process into myotubes is the extensive remodelling of the mitochondrial network. It has been proposed that, alterations in the remodelling of the mitochondrial network during the transition from proliferation to differentiation can lead to the diminished ability to regenerate muscle tissue [72]. Given the underlying reformation of the mitochondrial network during myogenesis, we aimed to analyse the mitochondrial function of differentiated satellite cells in the presence or absence of palmitate (i.e. a free fatty acid). During differentiation, the oxygen consumption rate (OCR) has been shown to increase significantly as a result of the elevated energy demand [73]. In line with previously published data [74] we report here, that isolated WT satellite cells show a significant increase of maximal oxygen consumption during the transition from proliferation to differentiation. However, CD36 KO derived satellite cells were unable to increase their OCR during the process of differentiation. This finding provides a plausible explanation for the impaired differentiation of satellite cells from CD36 KO animals reported in this study. Furthermore, treatment with palmitate-induced opposing effects between satellite cells isolates from WT and CD36 KO mice, resulting in increased OCR only in the WT, suggesting that CD36 is a key regulator of β-oxidation in satellite cells [75]. It appears that impaired myogenic differentiation with palmitate under CD36 deficiency is not affected by ROS levels, but rather perturbed bioenergetics due to inability to increase OCR. This notion is strengthened by previous

evidence showing that palmitate-induced mtDNA damage in skeletal muscle cells had deleterious effects on mitochondrial respiration [76].

Here we show that CD36-deficiency impairs muscle regeneration following CTX injury, evidenced by an increased occurrence of necrotic fibres and reduced CSA in the injured muscle of CD36 KO mice. Along with this, our results show a significant decrease in macrophage infiltration in CD36 KO mice 5 days after CTX injury. This is in agreement with previous data showing impaired macrophage phagocytic capacity in cardiac tissue due to CD36 inhibition [77]. This notion is further supported by the attenuated phagocytosis seen in pharmacological inhibition of CD36 which plays an important role during tissue repair and the resolution of inflammation [78]. CD36 has been found to be crucial for M2 macrophage polarization, involved in the transition from the M1 (pro-inflammatory) to the anti-inflammatory response marked by M2 macrophages, indicating that CD36-mediated uptake of triacylglycerol is crucial for M2 activation [79]. In addition, recent data on reduced tissue infiltration of macrophages in a model of cell-restricted deletion of CD36 suggests an important immune-regulatory function of CD36 [80]. In fact, CD36 is involved in the signalling cascades that allow macrophages to recognise cells undergoing apoptosis. Recognition and attachment of macrophages to apoptotic cells further involves ROS-induced lipid and protein oxidation which suggests another important mediatory role of CD36 in ROS dependent macrophage-driven phagocytosis [81,82]. Collectively, these data show that CD36 plays a crucial role in macrophage tissue infiltration and ROS dependent recognition of apoptotic cells with a crucial role for the post-inflammatory resolution phase and debris removal, important for the regenerative process after acute skeletal muscle injury [78]. This outcome is in line with our *in vitro* data in this study, showing impaired differentiation capacity in satellite cells isolated from CD36 KO mice. Furthermore, we

found significantly reduced CSA in CD36 KO mice 10 days following CTX injection. This is followed by increased expression of eMHC in CD36 KO compared to WT mice, suggesting delayed regeneration 10 days after muscle injury. We demonstrate that the impaired regeneration seen *in vivo* is at least in part brought about by the reduced stem cell commitment to differentiation seen in isolated satellite cells.

CD36 deficiency is known to result in hyperlipidaemia under both standard or a high fat diet (**Supplementary Table 1**). The CD36 KO mouse maintained on a HF diet had decreased levels of fatty acid accumulation in the skeletal muscle, however, adverse effects were seen in the liver tissue, evidenced by large lipid-droplets associated with hepatic steatosis. These findings parallel previously published results showing that CD36 deficiency in mice increases skeletal muscle insulin sensitivity in skeletal muscle, but induces insulin resistance in the liver [83,84]. FATP1, a member of the FATP/Slc27 protein family, is an insulin-sensitive fatty acid transporter. It has been shown to translocate from the intracellular compartment to the plasma membrane in response to insulin and to be involved in the re-distribution of lipids from adipose and skeletal muscle tissue to the liver. A significant observation in the present study is that liver *Fatp1* mRNA contents are 2.3- and 3.6-fold higher in CD36 KO versus WT HF and WT ND mice respectively. We conclude that in CD36 deficient mice, upregulation of FATP1 plays a key role in the development of hepatic steatosis in the presence of elevated free fatty acid availability. Our findings mirror the observation made in human CD36 deficiency, showing impaired fatty acid uptake by the heart but no restriction in the liver [85,86]. It has been suggested that in CD36-deficient humans may lead to increased postprandial fatty acid uptake in tissues that do not depend on CD36, such as the liver, resulting in lipid overload and the development of insulin resistance [86].

Our findings identify FATP1 as a potential target to prevent lipid overload to the liver in CD36 deficiency.

Our investigations further revealed a more than 20-fold increase in the expression level of *Cidea* in liver from CD36 KO mice on a high-fat diet compared to WT HF fed animals. *Cidea* is involved in energy expenditure and obesity and has been described to inhibit lipolysis [41]. *Cidea* KO mice exhibit higher energy expenditure, increased lipolysis in brown adipose tissue and are resistant to HF diet-induced obesity [87]. This supports our interpretation that CD36-deficient mice develop hepatic steatosis since it is known that *Cidea* positively correlates with lipid droplet enlargement, fusion and the development of fatty liver disease [88]. The development of non-alcoholic fatty liver disease (NAFLD) is one of the many complications associated with obesity and the development of diabetes. Here we report an important link between CD36 and *Cidea* with potential implications in the management of NAFLD. Furthermore, CD36 expression has been shown to be associated with tissue inflammation [89] and increased oxidative stress [33]. In the present study we show that markers of oxidative stress in skeletal muscle are reduced, paralleled by increased antioxidant enzyme gene expression in CD36-deficient mice under HF-diet, suggesting improved redox homeostasis. These findings are in line with recently published data showing decreased obesity-associated oxidative stress in the hearts of CD36-deficient mice [33].

In conclusion, we show that CD36-deficiency protects mice from diet-induced weight-gain. CD36 KO mice on a HF diet demonstrated decreased skeletal muscle lipid accumulation, suggesting CD36 as an important link between lipotoxicity and oxidative stress in obesity. Our study provides new insights for the involvement of CD36 in the development of hepatic steatosis, establishing *Fatp1* and *Cidea* as potential therapeutic targets. This study further elucidates the complexity of the underlying

alterations in mitochondrial fatty acid oxidation and bioenergetics related to obesity, supporting evidence of the contribution of CD36 to the development of the metabolic syndrome. Most importantly, CD36-deficient mice exhibited impaired satellite cell differentiation and skeletal muscle regeneration, which identifies CD36 as a key regulator of these processes. Further research will be necessary to clarify the underlying mechanism of impaired skeletal muscle regeneration in the absence of CD36 to provide a basis to better understand the link between CD36-mediated skeletal muscle lipid metabolism in the context of muscle regeneration in obesity.

Figure legends

Figure 1. CD36-deficient mice show reduced body weight gain upon high-fat diet compared to wild-type mice. (**A**) Schematic outline of dietary intervention and single muscle fibre isolation for muscle stem cell cultures in subsequent experiments; control diet (ND), high-fat (HF) diet in Wild-type (WT) and CD36 Knockout (KO) mice. (**B**) Representative images of WT and CD36 KO mice subjected to a ND and HF diet. (**C**) Body weight changes in WT and CD36 KO mice fed a ND or a HF diet for 13 weeks. (**D**) Final body weight (i.e. week 13) of mice fed a ND or HF diet. Data are mean±SD (N=8 per group). Statistical analysis was performed by three-way ANOVA, *p<0.05 *vs.* WT ND, $^{\#}$p<0.05 *vs.* WT HF.

Figure 2. Effect of CD36 deficiency and high-fat diet on lipid accumulation in skeletal muscle. (**A**) Skeletal muscle lipid accumulation in WT and CD36 KO mice on either ND or HF diet was detected by BODIPY staining (20x, scale bar=100µm). (**B**) Quantification of fluorescence intensity shown in arbitrary units (a.u.) of pixel intensity. **(C)** Gas chromatography was performed in skeletal muscle, quantifying the triacylglycerol (TG) and phospholipid (PL) content (µmol/g). **(D)** Relative gene expression in skeletal muscle was analysed by qRT-PCR. Data are mean±SD (N=6) per group. Statistical analysis was performed by two-way ANOVA, *p<0.05 *vs.* WT ND, $^{\#}$p<0.05 *vs.* WT HF ^{b}p<0.05 *vs.* CD36KO ND, $^{\$}$p<0.05.

Figure 3. CD36 deficiency attenuates high-fat diet-induced protein modification and increases antioxidant gene expression in skeletal muscle. **(A)** Skeletal muscle lipid peroxidation was analysed using TBARS. **(B-D)** Skeletal muscle oxidative protein modification for 4-HNE adducts and 3NT was assessed in quadriceps (QD) muscle by western blotting. **(E-F)** Relative gene expression in skeletal muscle for genes involved in DNA repair and redox equilibrium. **(G)** Representative images of

DHE staining to assess ROS production in isolated satellite cells, cultured in differentiation medium for 5 days in the absence or presence of palmitate (PA). **(H)** Quantification of total DHE^{+ve} nuclei/total DAPI, DHE^{+ve} nuclei/myotube/total DAPI and nuclear size (μm^2) with *p<0.05 vs. all other experimental groups. Data are represented as mean±SD (N=5-6) per group. Statistical analysis was performed using two-way ANOVA, *p<0.05 *vs.* WT ND, $^{\#}$p<0.05 *vs.* WT HF, ^{b}p<0.05 *vs.* CD36 KO ND, $^{¥}$p<0.05 *vs.* every other group.

Figure 4. High-fat diet and CD36 deficiency independently attenuate satellite cell proliferation on single fibres. (A) Representative pictures show EDL satellite cell immunostaining for Pax7 and Myogenin counterstained with DAPI. **(B-C)** Quiescent satellite cells were identified 0 h (0 hours) and quantified using immunostaining for Pax7. Satellite cell proliferation after 24 h and 48 h (24 and 48 hours) was quantified by Pax7 and MyoD, and differentiation after 72 h (72 hours) by Pax7 and Myogenin immunostaining. **(D)** Myonuclei to satellite cell (SC) ratio of the myofibres for WT and CD36 KO mice fed ND of HF at 0 h. Data are represented as mean±SEM (N=8 mice per condition; 50-70 individual myofibres were counted). Statistical analysis was performed using two-way ANOVA, *p<0.05 *vs.* WT ND, $^{\#}$p<0.05 *vs.* every other group.

Figure 5. CD36 is important for satellite cell differentiation and skeletal myogenesis. Immunohistochemistry was performed on isolated, plated satellite cells from EDL and BB in proliferation medium (PM) and cultured in growth medium (GM). **(A)** Schematic of satellite cell isolation-protocol from muscle tissue. **(B)** Differentiation was quantified after changing the GM to differentiation medium (DM) for 5 subsequent days. Satellite cells were immunostained for Myogenin and nuclei counterstained using DAPI. Differentiation was determined as Myogenin/DAPI (%) and the fusion index as $Myogenin^{+ve}$ nuclei inside myotubes divided by total DAPI. **(C)** Relative gene

expression by qRT-PCR for genes regulating skeletal myogenesis. Data are represented as mean±SD (N=3-4 technical replicates, 2 independent experiments) per group. Statistical analysis was performed using Student's *t*-tests or two-way ANOVA as appropriate, *p<0.05.

Figure 6. Palmitate impairs satellite cell differentiation in WT and CD36 deficient satellite cells. (A) Immunohistochemistry was performed on isolated satellite cells derived from WT or CD36 KO mice, that had been transferred from growth medium (GM) to differentiation medium (DM) to induce differentiation (scale bar=200μm). **(A-C)** Following expansion in GM, differentiation was quantified after 5 days in DM with DMSO (control) or palmitate (PA) and/or SSO (CD36 inhibition). Satellite cells were immunostained for Myogenin and nuclei counterstained using DAPI to quantify total cell numbers. **(B)** Quantification of Myogenin^{+ve} nuclei inside myoblasts and myotubes as a ratio to total DAPI (Myogenin/DAPI ratio. **(C)** Fusion Index (%) was assessed by Myogenin^{+ve} nuclei inside myotubes divided by total DAPI. Data are represented as mean±SD (N=3-4 technical replicates, 3 independent experiments) per group. Statistical analysis was performed using two-way ANOVA, *p<0.05 vs WT.

Figure 7. CD36 deficiency and increased fatty acid availability affect the metabolic profile of satellite cells. Respiration rate of isolated satellite cells was measured using the Seahorse XFp extracellular flux analyser. **(A)** Schematic of Seahorse Extracellular Flux Analysis set up. **(B-C)** Proliferating satellite cells from WT and CD36 KO mice were cultured in a seahorse extracellular flux cell culture plate. **(D-E)** Differentiated satellite cells from WT and CD36 KO mice were cultured in a seahorse extracellular flux cell culture plate and treated with SSO and/or palmitate before subsequent OCR measurements. In total, 13 OCR measurements were taken. Measurements are as follows: 3 basal respiration, 3 after the injection of Oligomycin

(Inhibition of ATP synthesis), 5 after the injection of FCCP (Uncoupling of ATP synthesis) and 2 after the injection of Antimycin (Inhibition of mitochondrial respiration). The x-axis represents measurements taken over a time interval of 2 hours and OCR values are represented as a mean of 3 independent measurements, shown on the y-axis. OCR values were normalised to total protein content and OCR changes are shown as pmol/min/µg total protein. Data are represented as mean±SD (N=3 independent experiments). Statistical analysis was performed using two-way ANOVA or Student's *t*-test as appropriate, *p<0.05 *vs.* WT, $^{\#}$p<0.05 *vs.* WT+PA, ^{b}p<0.05 *vs.* CD36KO.

Figure 8. CD36-deficiency impairs skeletal muscle regeneration after cardiotoxin-induced injury in tibialis anterior. (**A-B**) Representative images for the identification of regenerating fibres (haematoxylin & eosin staining, eMHC expression), damaged/dying fibres (IgG expression) and intramuscular macrophages (CD68) in muscle sections on day 5- and 10- post CTX injury (20x, scale bar=100µm). Quantification of CSA distribution from eMHC^{+ve} stained muscle fibres (D5 and D 10) and eMHC^{+ve} fibre number (D10, arrowheads), IgG staining inside the muscle fibres and CD68 are shown. Data are represented as mean±SD (N=5 per group). Statistical analysis was performed by Student's *t*-test or chi square test as appropriate with *p<0.05 and $^{\$}$p<0.05 *vs.* WT.

Figure 9. Effect of CD36 deficiency and high-fat diet on lipid accumulation in the liver. **(A)** Liver lipid accumulation was detected by Oil red O staining in cross-sections (20x, scale bar=100µm). **(B)** Quantification of lipid droplet distribution versus size. **(C)** Triacylglycerol (TG) and phospholipid (PL) contents (µmol/g) in the liver were quantified by gas chromatography. **(D)** Relative gene expression in the liver for genes involved in fatty acid metabolism and lipid fusion was analysed by qRT-PCR. Data are

mean±SD (N=6) per group. Statistical analysis was performed by two-way ANOVA, *p<0.05 *vs.* WT ND, #p<0.05 *vs.* WT HF bp<0.05 *vs.* CD36KO ND. Lipid droplet distribution was analysed by chi square, $p<0.01 *vs.* CD36KO ND, &p<0.05 *vs.* WT HF.

Acknowledgements

AM was funded by the by the European Union (Grant: FP7-PEOPLE-PCIG14-GA-2013-631440) and KP was funded by the BBSRC (BB/J016454/1).

The authors declare no conflict of interest.

Supplementary data

Supplementary Table 1. Overview of the effect of CD36 deficiency on blood lipids and glucose

	CD36 KO ND vs. WT ND	CD36 KO HF vs. WT HF
Total Cholesterol	**↑0- 1.3fold** (Febbraio, M. et al. 1999 PMID: 10383407 Goudriaan et al . 2003 PMID12923231, Brundert et al. 2011 PMID3284166)	No difference (Berger et al. 2019 PMID31289200)
VLDL/IDL	**↑1.4 fold** (Masuda, D. et al. 2008 PMID: 2666186,	**↑3fold** (Masuda, D. et al. 2008 PMID: 2666186)
LDL	No difference (Masuda, D. et al. 2008 PMID: 2666186	**↑2-fold** (Masuda, D. et al. 2008 PMID: 2666186)
TGs	**↑1.3fold- 2.4fold** (Jeltje R. Goudriaan et al. 2005 PMID: 16024917, Febbraio, M. et al. 1999 PMID: 10383407, Coburn et al. 2000 PMID: 10913136, Masuda, D. et al. 2008 PMID: 2666186, Goudriaan et al . 2003 PMID12923231, Hajri et al 2002 PMID150975)	**↑1.3fold** (Jeltje R. Goudriaan et al. 2005 PMID: 16024917, Hajri et al 2002 PMID150975)
FFA	**↑1.4- 1.9 fold** (Febbraio, M. et al. 1999 PMID: 10383407, (Masuda, D. et al. 2008 PMID: 2666186, Jeltje R. Goudriaan et al. 2005 PMID: 16024917, Goudriaan et al . 2003 PMID12923231, Hajri et al 2002 PMID150975	**↑1.4-2fold** (Masuda, D. et al. 2008 PMID: 2666186, Koonen et al. 2010 PMID2874697, Hajri et al 2002 PMID150975
Glucose	**↓0.5- 0.7fold** Goudriaan et al . 2003 PMID12923231, Hajri et al 2002 PMID150975	**↓1.8- 1.9 fold** Koonen et al. 2010 PMID2874697, Hajri et al 2002 PMID150975

Supplementary figure legends

Supplementary Figure 1. Tissue weight differences in Wild-type and CD36 deficient mice. **(A)** Soleus (Sol), **(B)** Biceps Brachii (BB), **(C)** Extensor digitorum longus (EDL), **(D)** Tibialis Anterior (TA), **(E)** heart and **(F)** White-Adipose-Tissue (WAT) from WT and CD36 KO mice fed a ND or a HF diet. Data are represented as mean±SD (N=8 per group). Statistical analysis was performed using two-way ANOVA, *p<0.05 *vs.* WT ND, #p <0.05 *vs.* WT HF, ^{b}p<0.05 *vs.* CD36 KO ND.

Supplementary Figure 2. CD36 deficiency alters diet induced muscle specific adaptations/morphometric changes. **(A, E)** Representative images of cross-sections from WT and CD36 KO mice fed a ND or HF diet from EDL and Sol muscle stained for myosin heavy chain (Mhc) isoforms. EDL and Sol muscle were examined for fibre type composition **(B, F)**, and cross-sectional area (CSA) **(C-D, G-H)**, respectively. EDL fibre type expression profile (IIA IIB IIX) and Soleus fibre type expression profile (IIA I IIX) shown in percentage [%]. Data are represented as mean±SD (N=8) per group). Statistical analysis was performed using two-way ANOVA or chi square analysis as appropriate, *p<0.05 vs WT ND.

Supplementary Figure 3. Attenuated DHE staining in the EDL muscle of CD36 KO mice. Representative images of DHE staining to assess ROS production in EDL transverse sections from WT and CD36 KO mice. Quantification of DHE staining intensity. Data are represented as mean±SD (N=6) per group. Statistical analysis was performed using Student's *t*-Test, *p<0.05.

Supplementary Figure 4. Compromised myogenic differentiation in CD36 KO skeletal myoblasts versus WT. Immunohistochemistry was performed on isolated satellite cells derived from WT or CD36 KO mice. Following expansion in growth medium, differentiation was quantified after 4 days in differentiation medium (x10 magnification, scale bar 100μm). Satellite cell differentiation and myotube formation was measured by Desmin, SRF and BEX1 and nuclei were counterstained with DAPI. Statistical analysis was performed by Student's *t*-test. Differences are *p<0.05.

Supplementary Fig. 5. The effect of high-fat diet and CD36 deficiency on MAPKs in skeletal muscle. Phosphorylation levels of various MAPKs were assessed in skeletal muscle of WT and CD36 KO mice fed a standard chow diet (normal diet, ND) or High-fat (HF) diet for 13 weeks. Results of Phospho-MAPK antibody array (R&D). The densitometric analysis was presented as fold change. Fold change was calculated as: the ratio of each of the 3 groups to WT ND group (n=6/group).

Supplementary Figure 6. Palmitate increases DHE levels and compromises muscle stem cell differentiation that can be reversed by antioxidants in WT mice, but not in CD36 KO. (A) Immunohistochemistry was performed on isolated satellite cells derived from WT or CD36 KO mice. Following expansion in growth medium (GM), differentiation was quantified after 4 days in differentiation medium (DM) with DMSO (control), Palmitate, Palmitate + Ebselen (20μM), or Palmitate + TEMPOL (1mM). Satellite cells were immunostained for MHC, DHE and nuclei counterstained using DAPI (Magnification x20, scale bar 50μm). **(B)** Quantification of DHE and MHC staining intensity (A.U.). Data are represented as mean±SD (N=6 technical replicates,

2 independent experiments) per group. Statistical analysis was performed using two-way ANOVA, *p<0.05 *vs* WT, #p<0.05 *vs* every other WT group.

Supplementary Figure 7. Palmitate increases DHE levels and compromises muscle stem cell differentiation that is reversible by the antioxidant agent ebselen in WT, but not in CD36 KO single fibre cultures. (A) Representative images show WT and CD36 KO EDL satellite cell staining for DHE and Myogenin counterstained with DAPI on single myofibres after 72 h (72 hours) treated with Palmitate (0.3mM) and/or Ebselen (20μM). **(B)** Quantification of DHE levels and Myogenin. Data are represented as mean±SD (N=5 mice per condition, 40 fibres per group). Statistical analysis was performed using two-way ANOVA, *p<0.05 *vs.* WT ND, #p<0.05 *vs.* every other WT group.

Supplementary Figure 8. The effect of CD36 deficiency on MyoD and Myogenin expression in progenitor cells of injured muscle. Acute injury was induced by Cardiotoxin injection into the tibialis anterior muscle of WT and CD36 KO mice and specimens were studied 5 days post-injury. Representative images and quantitative data for MyoD and Myogenin immunohistochemical staining on transverse sections of injured muscles, co-stained with DAPI to visualise nuclei. Representative images (x20 magnification, scale bar 50μm). Statistical analysis was performed by Student's *t*-test. n=5 animals per group. Differences are *p<0.05.

References

1. MAURO A. Satellite cell of skeletal muscle fibers. *J Biophys Biochem Cytol.* 1961;9:493-495.
2. Montarras D, Morgan J, Collins C, et al. Direct isolation of satellite cells for skeletal muscle regeneration. *Science.* 2005;309(5743):2064-2067.
3. Shea KL, Xiang W, LaPorta VS, et al. Sprouty1 regulates reversible quiescence of a self-renewing adult muscle stem cell pool during regeneration. *Cell Stem Cell.* 2010;6(2):117-129.
4. Zammit PS, Relaix F, Nagata Y, et al. Pax7 and myogenic progression in skeletal muscle satellite cells. *J Cell Sci.* 2006;119(Pt 9):1824-1832.
5. Dumont NA, Wang YX, von Maltzahn J, et al. Dystrophin expression in muscle stem cells regulates their polarity and asymmetric division. *Nat Med.* 2015;21(12):1455-1463.
6. Rozo M, Li L, Fan CM. Targeting β1-integrin signaling enhances regeneration in aged and dystrophic muscle in mice. *Nat Med.* 2016;22(8):889-896.
7. D'Souza DM, Trajcevski KE, Al-Sajee D, et al. Diet-induced obesity impairs muscle satellite cell activation and muscle repair through alterations in hepatocyte growth factor signaling. *Physiol Rep.* 2015;3(8).
8. Sinha I, Sakthivel D, Olenchock BA, et al. Prolyl Hydroxylase Domain-2 Inhibition Improves Skeletal Muscle Regeneration in a Male Murine Model of Obesity. *Front Endocrinol (Lausanne).* 2017;8:153.
9. Nguyen MH, Cheng M, Koh TJ. Impaired muscle regeneration in ob/ob and db/db mice. *ScientificWorldJournal.* 2011;11:1525-1535.
10. Fu X, Zhu M, Zhang S, Foretz M, Viollet B, Du M. Obesity Impairs Skeletal Muscle Regeneration Through Inhibition of AMPK. *Diabetes.* 2016;65(1):188-200.
11. Brown LA, Lee DE, Patton JF, et al. Diet-induced obesity alters anabolic signalling in mice at the onset of skeletal muscle regeneration. *Acta Physiol (Oxf).* 2015;215(1):46-57.
12. Akhmedov D, Berdeaux R. The effects of obesity on skeletal muscle regeneration. *Front Physiol.* 2013;4:371.
13. Kahn BB, Flier JS. Obesity and insulin resistance. *J Clin Invest.* 2000;106(4):473-481.
14. Hilton TN, Tuttle LJ, Bohnert KL, Mueller MJ, Sinacore DR. Excessive adipose tissue infiltration in skeletal muscle in individuals with obesity, diabetes mellitus, and peripheral neuropathy: association with performance and function. *Phys Ther.* 2008;88(11):1336-1344.
15. Gueugneau M, Coudy-Gandilhon C, Théron L, et al. Skeletal muscle lipid content and oxidative activity in relation to muscle fiber type in aging and metabolic syndrome. *J Gerontol A Biol Sci Med Sci.* 2015;70(5):566-576.
16. Unger RH, Clark GO, Scherer PE, Orci L. Lipid homeostasis, lipotoxicity and the metabolic syndrome. *Biochim Biophys Acta.* 2010;1801(3):209-214.
17. Bonen A, Han XX, Habets DD, Febbraio M, Glatz JF, Luiken JJ. A null mutation in skeletal muscle FAT/CD36 reveals its essential role in insulin- and AICAR-stimulated fatty acid metabolism. *Am J Physiol Endocrinol Metab.* 2007;292(6):E1740-1749.
18. Cameron-Smith D, Burke LM, Angus DJ, et al. A short-term, high-fat diet up-regulates lipid metabolism and gene expression in human skeletal muscle. *Am J Clin Nutr.* 2003;77(2):313-318.
19. Koonen DP, Sung MM, Kao CK, et al. Alterations in skeletal muscle fatty acid handling predisposes middle-aged mice to diet-induced insulin resistance. *Diabetes.* 2010;59(6):1366-1375.
20. Aguer C, Mercier J, Man CY, et al. Intramyocellular lipid accumulation is associated with permanent relocation ex vivo and in vitro of fatty acid translocase (FAT)/CD36 in obese patients. *Diabetologia.* 2010;53(6):1151-1163.
21. Ouwens DM, Diamant M, Fodor M, et al. Cardiac contractile dysfunction in insulin-resistant rats fed a high-fat diet is associated with elevated CD36-mediated fatty acid uptake and esterification. *Diabetologia.* 2007;50(9):1938-1948.

22. Glatz JF, Angin Y, Steinbusch LK, Schwenk RW, Luiken JJ. CD36 as a target to prevent cardiac lipotoxicity and insulin resistance. *Prostaglandins Leukot Essent Fatty Acids.* 2013;88(1):71-77.
23. Han XX, Chabowski A, Tandon NN, et al. Metabolic challenges reveal impaired fatty acid metabolism and translocation of FAT/CD36 but not FABPpm in obese Zucker rat muscle. *Am J Physiol Endocrinol Metab.* 2007;293(2):E566-575.
24. Bonen A, Parolin ML, Steinberg GR, et al. Triacylglycerol accumulation in human obesity and type 2 diabetes is associated with increased rates of skeletal muscle fatty acid transport and increased sarcolemmal FAT/CD36. *FASEB J.* 2004;18(10):1144-1146.
25. Knoblauch MA, O'Connor DP, Clarke MS. Obese mice incur greater myofiber membrane disruption in response to mechanical load compared with lean mice. *Obesity (Silver Spring).* 2013;21(1):135-143.
26. Kim J, So WY. High Body Mass Index Is Associated with the Extent of Muscle Damage after Eccentric Exercise. *Int J Environ Res Public Health.* 2018;15(7).
27. Xu P, Werner JU, Milerski S, et al. Diet-Induced Obesity Affects Muscle Regeneration After Murine Blunt Muscle Trauma-A Broad Spectrum Analysis. *Front Physiol.* 2018;9:674.
28. Matsakas A, Prosdocimo DA, Mitchell R, et al. Investigating mechanisms underpinning the detrimental impact of a high-fat diet in the developing and adult hypermuscular myostatin null mouse. *Skelet Muscle.* 2015;5:38.
29. Ingram KH, Hill H, Moellering DR, et al. Skeletal muscle lipid peroxidation and insulin resistance in humans. *J Clin Endocrinol Metab.* 2012;97(7):E1182-1186.
30. Pillon NJ, Croze ML, Vella RE, Soulère L, Lagarde M, Soulage CO. The lipid peroxidation by-product 4-hydroxy-2-nonenal (4-HNE) induces insulin resistance in skeletal muscle through both carbonyl and oxidative stress. *Endocrinology.* 2012;153(5):2099-2111.
31. Soulage CO, Sardón Puig L, Soulère L, et al. Skeletal muscle insulin resistance is induced by 4-hydroxy-2-hexenal, a by-product of n-3 fatty acid peroxidation. *Diabetologia.* 2018;61(3):688-699.
32. Sfyri PP, Yuldasheva NY, Tzimou A, et al. Attenuation of oxidative stress-induced lesions in skeletal muscle in a mouse model of obesity-independent hyperlipidaemia and atherosclerosis through the inhibition of Nox2 activity. *Free Radic Biol Med.* 2018;129:504-519.
33. Gharib M, Tao H, Fungwe TV, Hajri T. Cluster Differentiating 36 (CD36) Deficiency Attenuates Obesity-Associated Oxidative Stress in the Heart. *PLoS One.* 2016;11(5):e0155611.
34. Okamura DM, Pennathur S, Pasichnyk K, et al. CD36 regulates oxidative stress and inflammation in hypercholesterolemic CKD. *J Am Soc Nephrol.* 2009;20(3):495-505.
35. Furukawa S, Fujita T, Shimabukuro M, et al. Increased oxidative stress in obesity and its impact on metabolic syndrome. *J Clin Invest.* 2004;114(12):1752-1761.
36. Shinzawa K, Tsujimoto Y. PLA2 activity is required for nuclear shrinkage in caspase-independent cell death. *J Cell Biol.* 2003;163(6):1219-1230.
37. Kozakowska M, Pietraszek-Gremplewicz K, Jozkowicz A, Dulak J. The role of oxidative stress in skeletal muscle injury and regeneration: focus on antioxidant enzymes. *J Muscle Res Cell Motil.* 2015;36(6):377-393.
38. Handayaningsih AE, Iguchi G, Fukuoka H, et al. Reactive oxygen species play an essential role in IGF-I signaling and IGF-I-induced myocyte hypertrophy in C2C12 myocytes. *Endocrinology.* 2011;152(3):912-921.
39. Vannini N, Girotra M, Naveiras O, et al. Specification of haematopoietic stem cell fate via modulation of mitochondrial activity. *Nat Commun.* 2016;7:13125.
40. Yin H, Price F, Rudnicki MA. Satellite cells and the muscle stem cell niche. *Physiol Rev.* 2013;93(1):23-67.
41. Puri V, Ranjit S, Konda S, et al. Cidea is associated with lipid droplets and insulin sensitivity in humans. *Proc Natl Acad Sci U S A.* 2008;105(22):7833-7838.

42. Barneda D, Planas-Iglesias J, Gaspar ML, et al. The brown adipocyte protein CIDEA promotes lipid droplet fusion via a phosphatidic acid-binding amphipathic helix. *Elife.* 2015;4:e07485.
43. Febbraio M, Abumrad NA, Hajjar DP, et al. A null mutation in murine CD36 reveals an important role in fatty acid and lipoprotein metabolism. *J Biol Chem.* 1999;274(27):19055-19062.
44. Matsakas A, Macharia R, Otto A, et al. Exercise training attenuates the hypermuscular phenotype and restores skeletal muscle function in the myostatin null mouse. *Exp Physiol.* 2012;97(1):125-140.
45. Scully D, Sfyri P, Verpoorten S, et al. Platelet releasate promotes skeletal myogenesis by increasing muscle stem cell commitment to differentiation and accelerates muscle regeneration following acute injury. *Acta Physiol (Oxf).* 2019;225(3):e13207.
46. Petridou A, Nikolaidis MG, Matsakas A, Schulz T, Michna H, Mougios V. Effect of exercise training on the fatty acid composition of lipid classes in rat liver, skeletal muscle, and adipose tissue. *Eur J Appl Physiol.* 2005;94(1-2):84-92.
47. Xu J, Liu D, Yin H, Tong H, Li S, Yan Y. Fatty acids promote bovine skeletal muscle satellite cell differentiation by regulating ELOVL3 expression. *Cell Tissue Res.* 2018;373(2):499-508.
48. Taube A, Lamberndt S, van Echten-Deckert G, Eckardt K, Eckel J. Adipokines promote lipotoxicity in human skeletal muscle cells. *Arch Physiol Biochem.* 2012;118(3):92-101.
49. Cai L, Wang Z, Ji A, Meyer JM, van der Westhuyzen DR. Scavenger receptor CD36 expression contributes to adipose tissue inflammation and cell death in diet-induced obesity. *PLoS One.* 2012;7(5):e36785.
50. Hegarty BD, Cooney GJ, Kraegen EW, Furler SM. Increased efficiency of fatty acid uptake contributes to lipid accumulation in skeletal muscle of high fat-fed insulin-resistant rats. *Diabetes.* 2002;51(5):1477-1484.
51. Moors CC, van der Zijl NJ, Diamant M, Blaak EE, Goossens GH. Impaired insulin sensitivity is accompanied by disturbances in skeletal muscle fatty acid handling in subjects with impaired glucose metabolism. *Int J Obes (Lond).* 2012;36(5):709-717.
52. Goodpaster BH, Thaete FL, Kelley DE. Thigh adipose tissue distribution is associated with insulin resistance in obesity and in type 2 diabetes mellitus. *Am J Clin Nutr.* 2000;71(4):885-892.
53. Kurdiova T, Balaz M, Vician M, et al. Effects of obesity, diabetes and exercise on Fndc5 gene expression and irisin release in human skeletal muscle and adipose tissue: in vivo and in vitro studies. *J Physiol.* 2014;592(5):1091-1107.
54. Park SY, Yun Y, Kim IS. CD36 is required for myoblast fusion during myogenic differentiation. *Biochem Biophys Res Commun.* 2012;427(4):705-710.
55. Grabiec K, Milewska M, Błaszczyk M, Gajewska M, Grzelkowska-Kowalczyk K. Palmitate exerts opposite effects on proliferation and differentiation of skeletal myoblasts. *Cell Biol Int.* 2015;39(9):1044-1052.
56. Rotwein P, Wilson EM. Distinct actions of Akt1 and Akt2 in skeletal muscle differentiation. *J Cell Physiol.* 2009;219(2):503-511.
57. Ge Y, Chen J. Mammalian target of rapamycin (mTOR) signaling network in skeletal myogenesis. *J Biol Chem.* 2012;287(52):43928-43935.
58. Jonak C, Mildner M, Klosner G, et al. The hsp27kD heat shock protein and p38-MAPK signaling are required for regular epidermal differentiation. *J Dermatol Sci.* 2011;61(1):32-37.
59. Knight JD, Kothary R. The myogenic kinome: protein kinases critical to mammalian skeletal myogenesis. *Skelet Muscle.* 2011;1:29.
60. Koo JH, Smiley MA, Lovering RM, Margolis FL. Bex1 knock out mice show altered skeletal muscle regeneration. *Biochem Biophys Res Commun.* 2007;363(2):405-410.
61. Samovski D, Sun J, Pietka T, et al. Regulation of AMPK activation by CD36 links fatty acid uptake to β-oxidation. *Diabetes.* 2015;64(2):353-359.

62. Fu X, Zhu MJ, Dodson MV, Du M. AMP-activated protein kinase stimulates Warburg-like glycolysis and activation of satellite cells during muscle regeneration. *J Biol Chem.* 2015;290(44):26445-26456.
63. Williamson DL, Butler DC, Alway SE. AMPK inhibits myoblast differentiation through a PGC-1alpha-dependent mechanism. *Am J Physiol Endocrinol Metab.* 2009;297(2):E304-314.
64. Thomson DM. The Role of AMPK in the Regulation of Skeletal Muscle Size, Hypertrophy, and Regeneration. *Int J Mol Sci.* 2018;19(10).
65. Fulco M, Cen Y, Zhao P, et al. Glucose restriction inhibits skeletal myoblast differentiation by activating SIRT1 through AMPK-mediated regulation of Nampt. *Dev Cell.* 2008;14(5):661-673.
66. Kelley DE, He J, Menshikova EV, Ritov VB. Dysfunction of mitochondria in human skeletal muscle in type 2 diabetes. *Diabetes.* 2002;51(10):2944-2950.
67. Mogensen M, Sahlin K, Fernström M, et al. Mitochondrial respiration is decreased in skeletal muscle of patients with type 2 diabetes. *Diabetes.* 2007;56(6):1592-1599.
68. Sparks LM, Xie H, Koza RA, et al. A high-fat diet coordinately downregulates genes required for mitochondrial oxidative phosphorylation in skeletal muscle. *Diabetes.* 2005;54(7):1926-1933.
69. Campbell SE, Tandon NN, Woldegiorgis G, Luiken JJ, Glatz JF, Bonen A. A novel function for fatty acid translocase (FAT)/CD36: involvement in long chain fatty acid transfer into the mitochondria. *J Biol Chem.* 2004;279(35):36235-36241.
70. Pfleger J, He M, Abdellatif M. Mitochondrial complex II is a source of the reserve respiratory capacity that is regulated by metabolic sensors and promotes cell survival. *Cell Death Dis.* 2015;6:e1835.
71. Lonergan T, Bavister B, Brenner C. Mitochondria in stem cells. *Mitochondrion.* 2007;7(5):289-296.
72. Sin J, Andres AM, Taylor DJ, et al. Mitophagy is required for mitochondrial biogenesis and myogenic differentiation of C2C12 myoblasts. *Autophagy.* 2016;12(2):369-380.
73. Zhang Y, Marsboom G, Toth PT, Rehman J. Mitochondrial respiration regulates adipogenic differentiation of human mesenchymal stem cells. *PLoS One.* 2013;8(10):e77077.
74. Agostini M, Romeo F, Inoue S, et al. Metabolic reprogramming during neuronal differentiation. *Cell Death Differ.* 2016;23(9):1502-1514.
75. Townsend KL, An D, Lynes MD, et al. Increased mitochondrial activity in BMP7-treated brown adipocytes, due to increased CPT1- and CD36-mediated fatty acid uptake. *Antioxid Redox Signal.* 2013;19(3):243-257.
76. Patková J, Anděl M, Trnka J. Palmitate-induced cell death and mitochondrial respiratory dysfunction in myoblasts are not prevented by mitochondria-targeted antioxidants. *Cell Physiol Biochem.* 2014;33(5):1439-1451.
77. Lindsey ML, Jung M, Yabluchanskiy A, et al. Exogenous CXCL4 infusion inhibits macrophage phagocytosis by limiting CD36 signalling to enhance post-myocardial infarction cardiac dilation and mortality. *Cardiovasc Res.* 2019;115(2):395-408.
78. Woo MS, Yang J, Beltran C, Cho S. Cell Surface CD36 Protein in Monocyte/Macrophage Contributes to Phagocytosis during the Resolution Phase of Ischemic Stroke in Mice. *J Biol Chem.* 2016;291(45):23654-23661.
79. Huang SC, Everts B, Ivanova Y, et al. Cell-intrinsic lysosomal lipolysis is essential for alternative activation of macrophages. *Nat Immunol.* 2014;15(9):846-855.
80. Nicholls HT, Kowalski G, Kennedy DJ, et al. Hematopoietic cell-restricted deletion of CD36 reduces high-fat diet-induced macrophage infiltration and improves insulin signaling in adipose tissue. *Diabetes.* 2011;60(4):1100-1110.
81. Tan HY, Wang N, Li S, Hong M, Wang X, Feng Y. The Reactive Oxygen Species in Macrophage Polarization: Reflecting Its Dual Role in Progression and Treatment of Human Diseases. *Oxid Med Cell Longev.* 2016;2016:2795090.

82. Chang MK, Bergmark C, Laurila A, et al. Monoclonal antibodies against oxidized low-density lipoprotein bind to apoptotic cells and inhibit their phagocytosis by elicited macrophages: evidence that oxidation-specific epitopes mediate macrophage recognition. *Proc Natl Acad Sci U S A.* 1999;96(11):6353-6358.
83. Goudriaan JR, Dahlmans VE, Teusink B, et al. CD36 deficiency increases insulin sensitivity in muscle, but induces insulin resistance in the liver in mice. *J Lipid Res.* 2003;44(12):2270-2277.
84. Nassir F, Adewole OL, Brunt EM, Abumrad NA. CD36 deletion reduces VLDL secretion, modulates liver prostaglandins, and exacerbates hepatic steatosis in ob/ob mice. *J Lipid Res.* 2013;54(11):2988-2997.
85. Hirano K, Kuwasako T, Nakagawa-Toyama Y, Janabi M, Yamashita S, Matsuzawa Y. Pathophysiology of human genetic CD36 deficiency. *Trends Cardiovasc Med.* 2003;13(4):136-141.
86. Hames KC, Vella A, Kemp BJ, Jensen MD. Free fatty acid uptake in humans with CD36 deficiency. *Diabetes.* 2014;63(11):3606-3614.
87. Zhou Z, Yon Toh S, Chen Z, et al. Cidea-deficient mice have lean phenotype and are resistant to obesity. *Nat Genet.* 2003;35(1):49-56.
88. Xu W, Wu L, Yu M, et al. Differential Roles of Cell Death-inducing DNA Fragmentation Factor-α-like Effector (CIDE) Proteins in Promoting Lipid Droplet Fusion and Growth in Subpopulations of Hepatocytes. *J Biol Chem.* 2016;291(9):4282-4293.
89. Febbraio M, Hajjar DP, Silverstein RL. CD36: a class B scavenger receptor involved in angiogenesis, atherosclerosis, inflammation, and lipid metabolism. *J Clin Invest.* 2001;108(6):785-791.

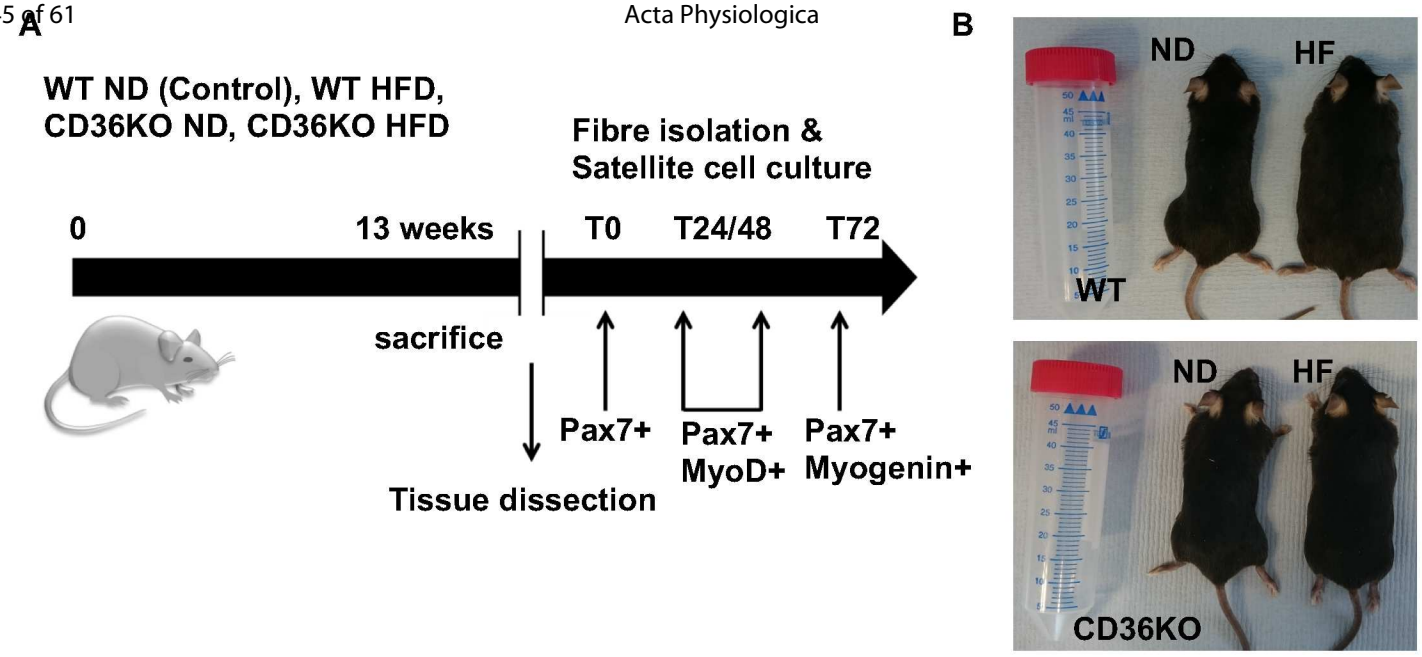
A
WT ND (Control), WT HFD,
CD36KO ND, CD36KO HFD
Fibre isolation &
Satellite cell culture
0
13 weeks
T0
T24/48
T72
sacrifice
Pax7+
Pax7+
MyoD+
Pax7+
Myogenin+
Tissue dissection
B
ND
HF
WT
ND
HF
CD36KO

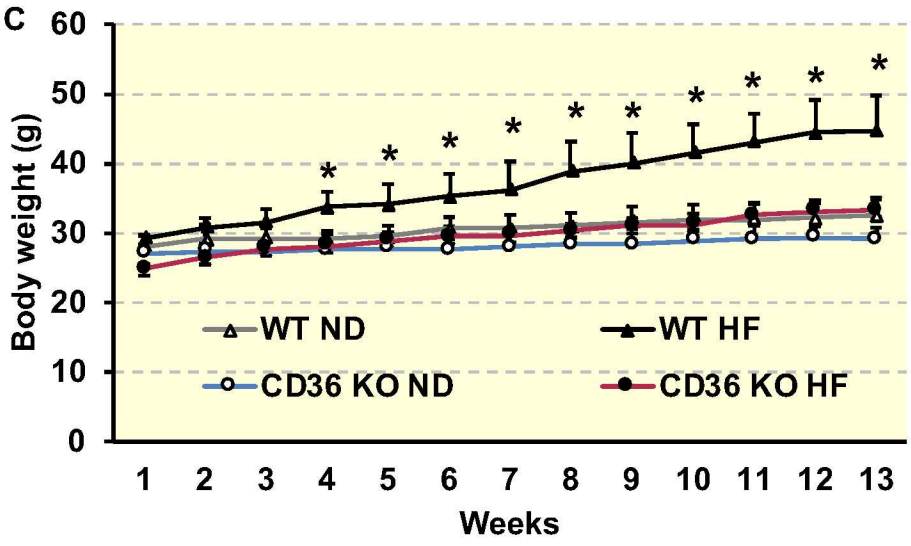
C
Body weight (g)
60
50
40
30
20
10
0
WT ND
WT HF
CD36 KO ND
CD36 KO HF
1 2 3 4 5 6 7 8 9 10 11 12 13
Weeks

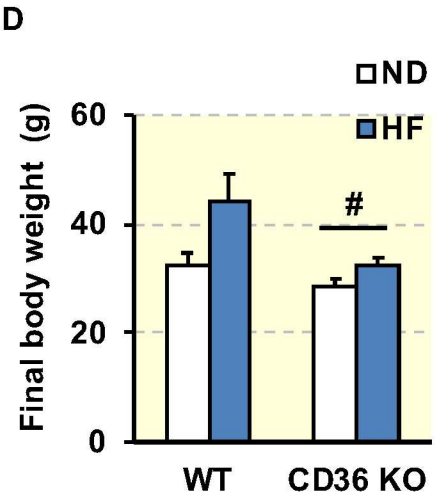
D
ND
HF
Final body weight (g)
60
40
20
0
#
WT
CD36 KO

Figure 1

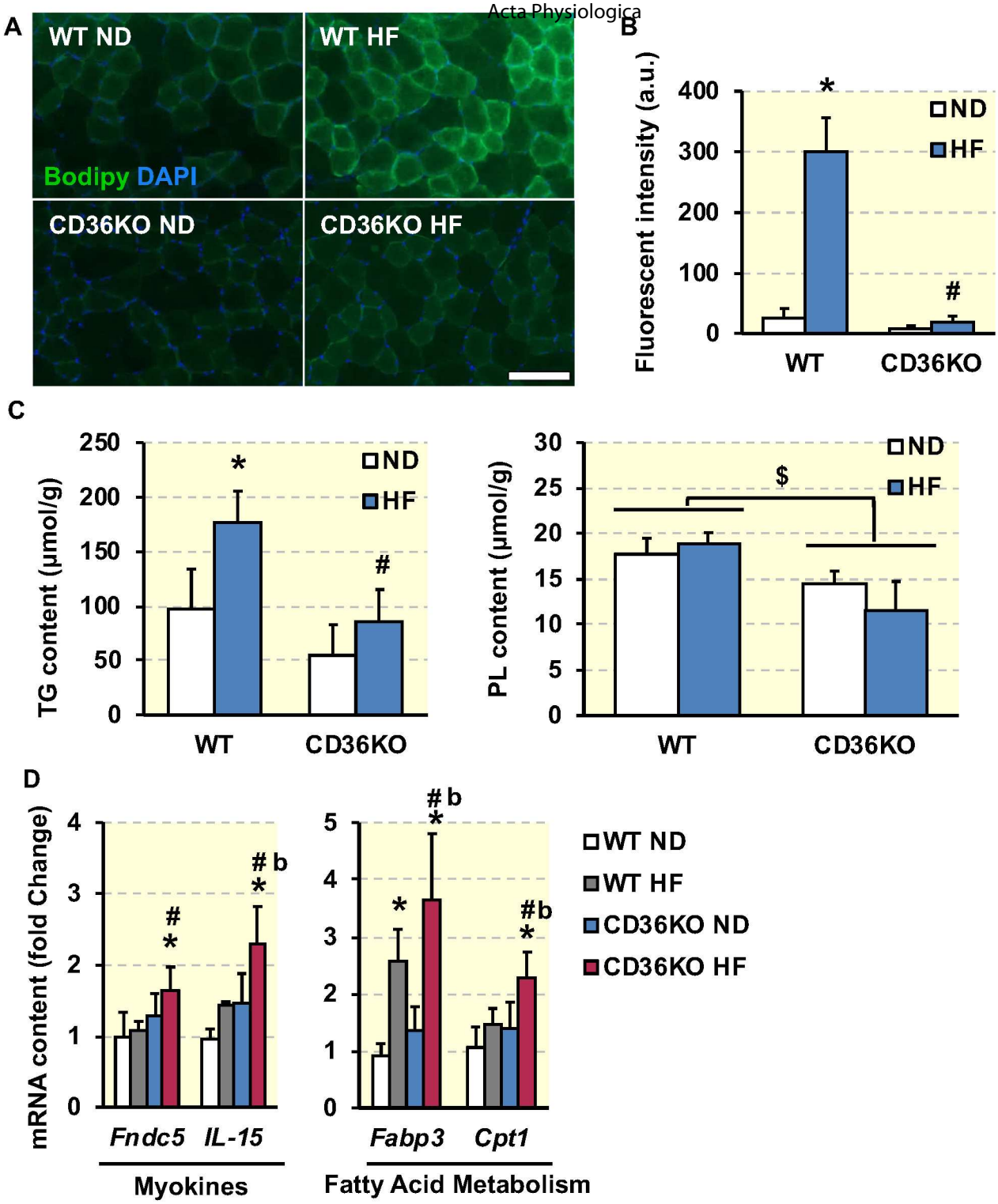
A
WT ND
WT HF
Bodipy DAPI
CD36KO ND
CD36KO HF
B
Fluorescent intensity (a.u.)
400
300
200
100
0
ND
HF
*
#
WT
CD36KO
C
TG content (µmol/g)
250
200
150
100
50
0
ND
HF
*
#
WT
CD36KO
PL content (µmol/g)
30
25
20
15
10
5
0
ND
HF
$
WT
CD36KO
D
mRNA content (fold Change)
4
3
2
1
0
b
*
#
*
Fndc5
IL-15
Myokines
5
4
3
2
1
0
b
*
*
#b
*
Fabp3
Cpt1
Fatty Acid Metabolism
WT ND
WT HF
CD36KO ND
CD36KO HF

Figure 2

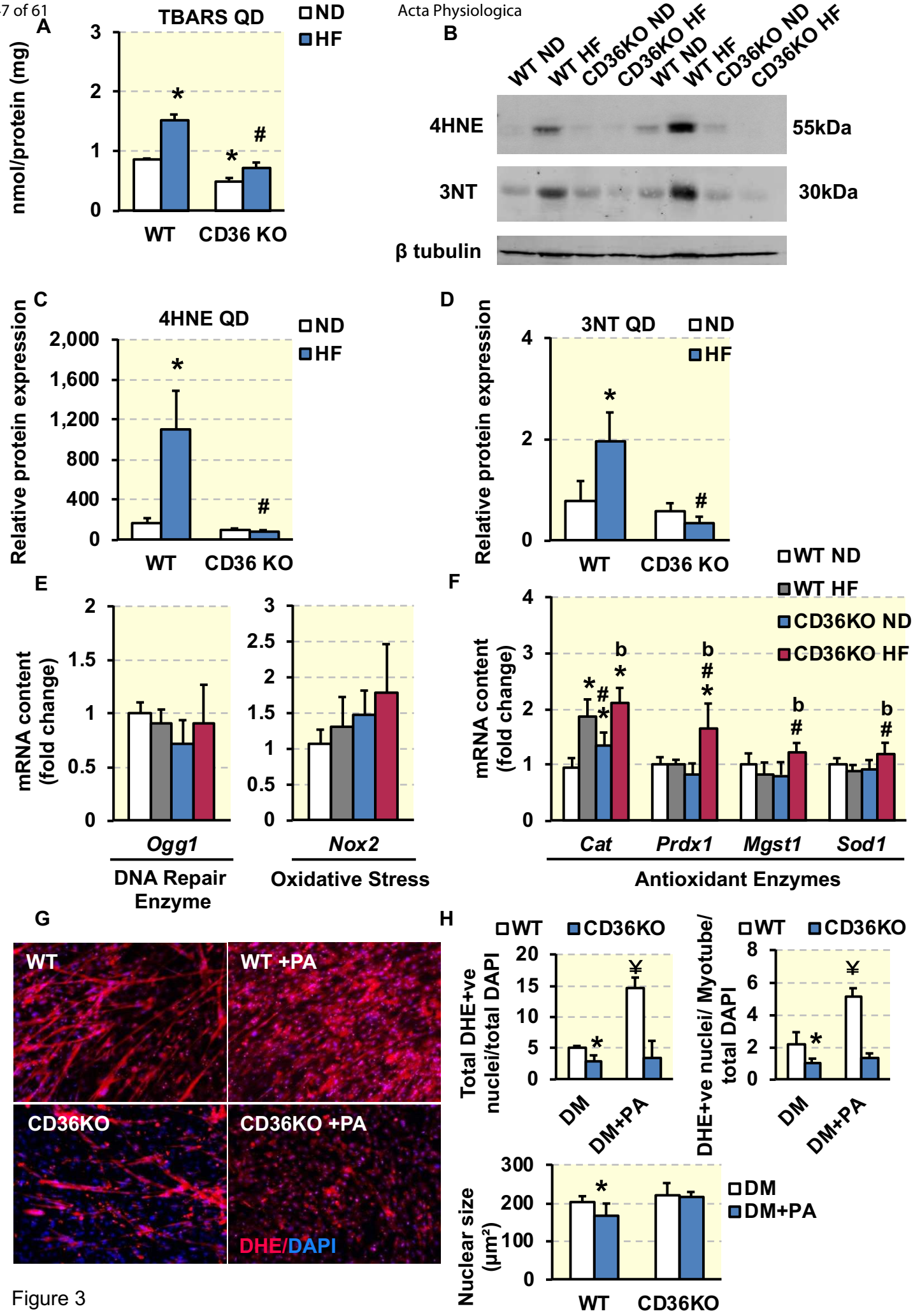
A
TBARS QD
ND
HF
nmol/protein (mg)
WT
CD36 KO
B
WT ND
WT HF
CD36KO ND
CD36KO HF
4HNE
55kDa
3NT
30kDa
β tubulin
C
4HNE QD
Relative protein expression
D
3NT QD
E
mRNA content (fold change)
Ogg1
Nox2
DNA Repair Enzyme
Oxidative Stress
F
Cat
Prdx1
Mgst1
Sod1
Antioxidant Enzymes
G
WT
WT +PA
CD36KO
CD36KO +PA
DHE/DAPI
H
Total DHE+ve nuclei/total DAPI
DHE+ve nuclei/ Myotube/ total DAPI
DM
DM+PA
Nuclear size (μm²)

Figure 3

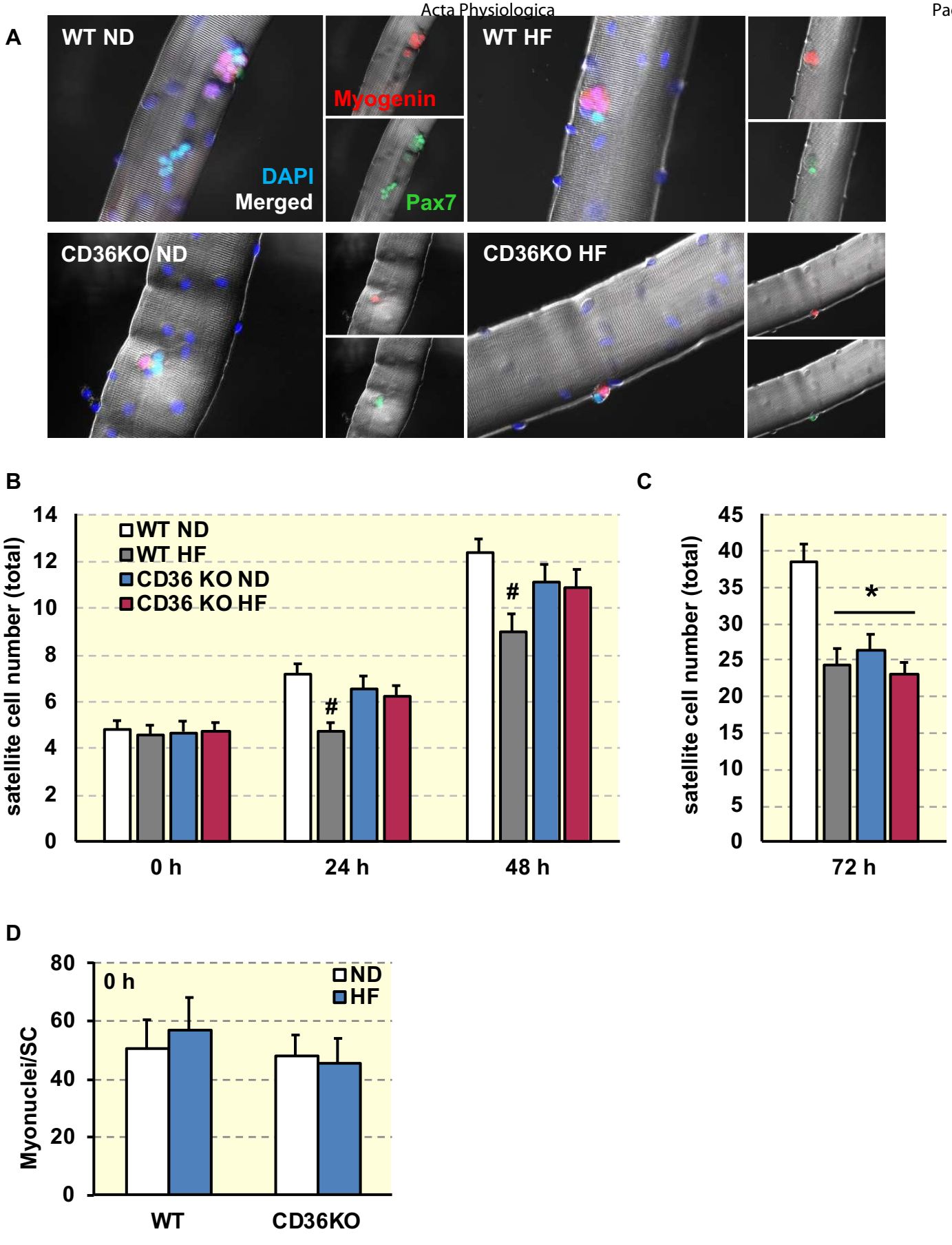
A
WT ND
DAPI
Merged
Myogenin
Pax7
WT HF
CD36KO ND
CD36KO HF
B
satellite cell number (total)
WT ND
WT HF
CD36 KO ND
CD36 KO HF
#
#
0 h
24 h
48 h
C
satellite cell number (total)
*
72 h
D
Myonuclei/SC
0 h
ND
HF
WT
CD36KO

Figure 4

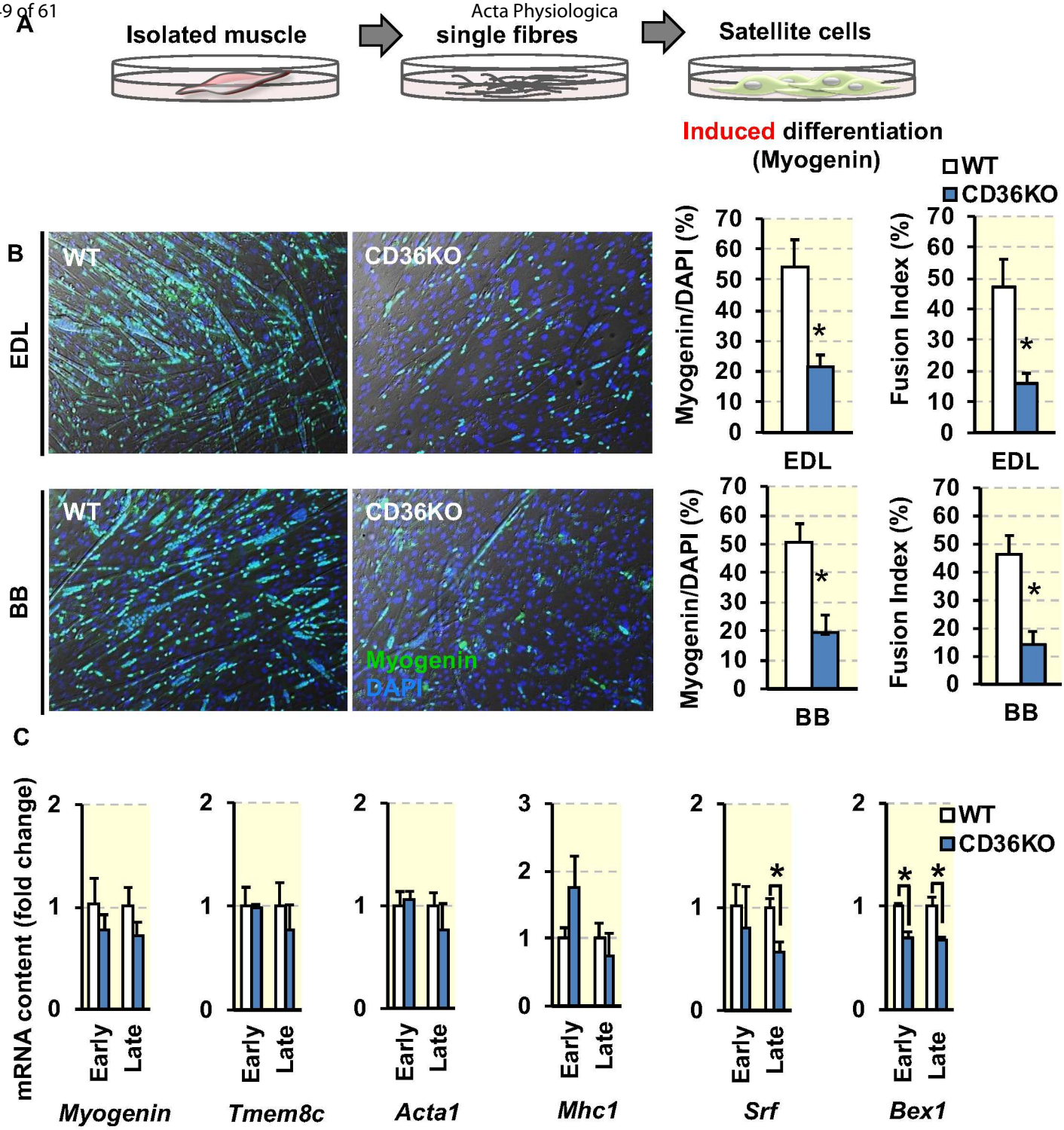
A
Isolated muscle
single fibres
Satellite cells
Induced differentiation
(Myogenin)
WT
CD36KO
B
EDL
BB
WT
CD36KO
Myogenin
DAPI
Myogenin/DAPI (%)
Fusion Index (%)
EDL
BB
C
mRNA content (fold change)
Early
Late
Myogenin
Tmem8c
Acta1
Mhc1
Srf
Bex1

Figure 5

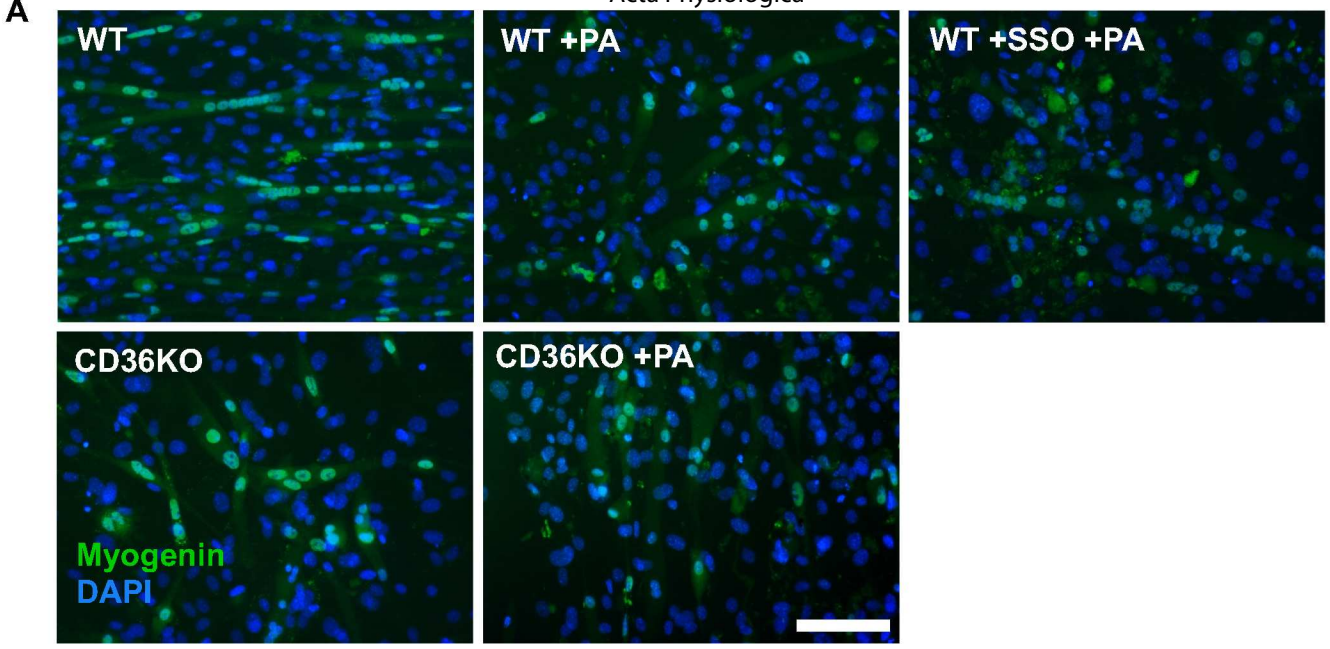
A
WT
WT +PA
WT +SSO +PA
CD36KO
CD36KO +PA
Myogenin
DAPI

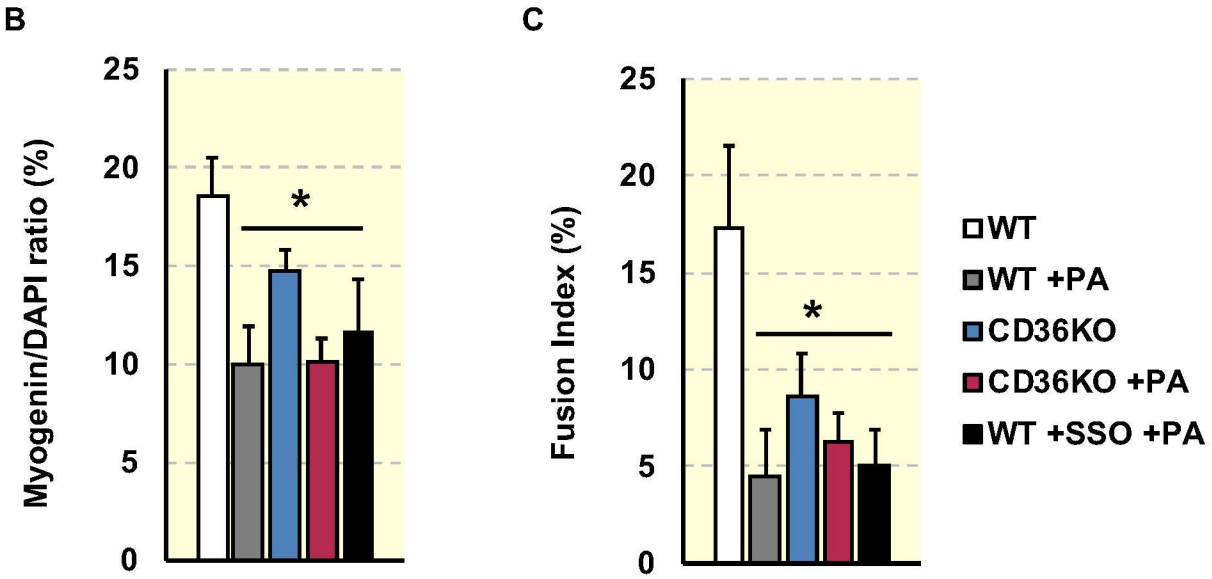
B
Myogenin/DAPI ratio (%)
25
20
15
10
5
0
*
C
Fusion Index (%)
25
20
15
10
5
0
*
WT
WT +PA
CD36KO
CD36KO +PA
WT +SSO +PA

Figure 6

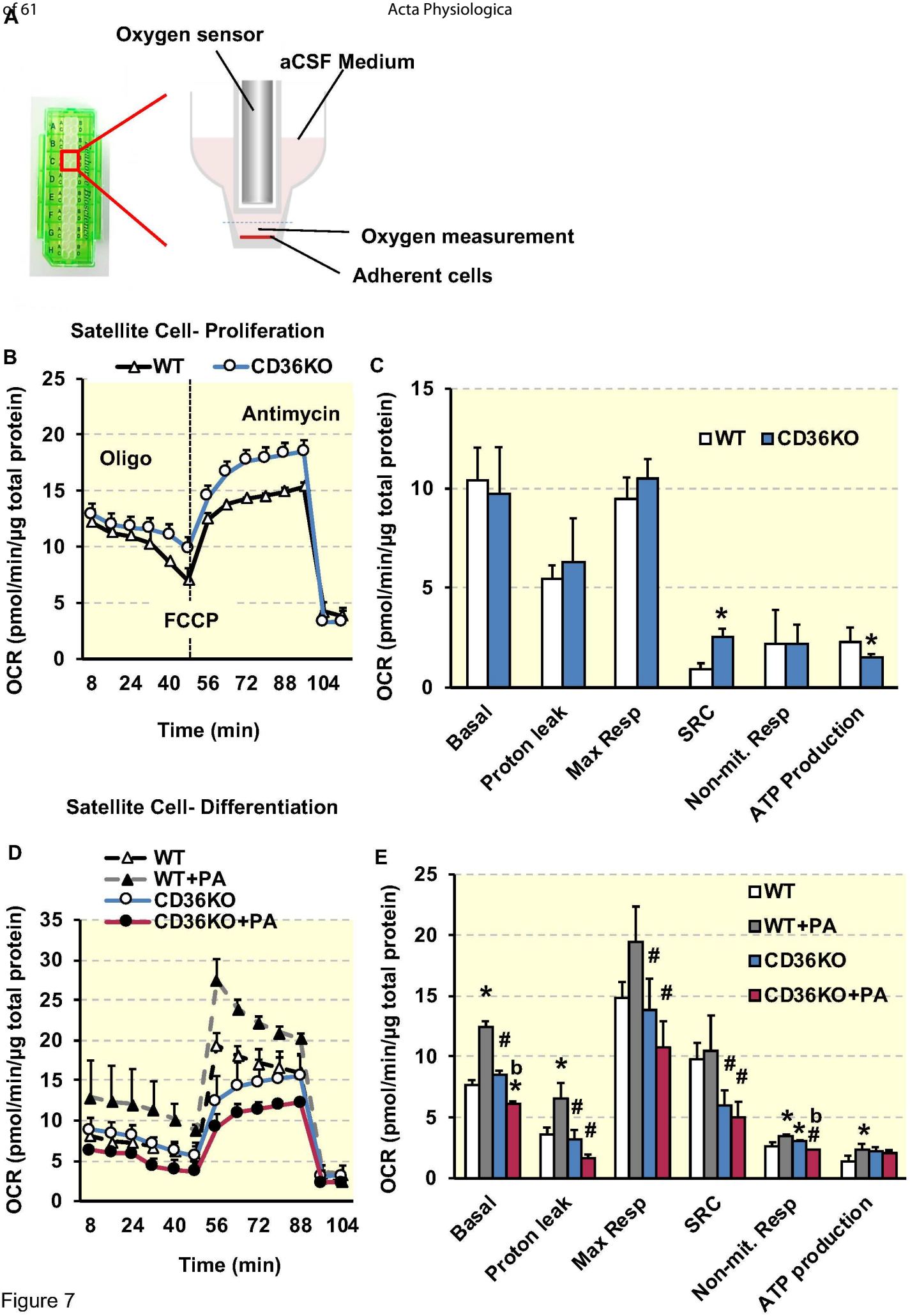
A
Oxygen sensor
aCSF Medium
Oxygen measurement
Adherent cells
Satellite Cell- Proliferation
B
WT
CD36KO
Antimycin
Oligo
FCCP
OCR (pmol/min/µg total protein)
Time (min)
C
WT
CD36KO
Basal
Proton leak
Max Resp
SRC
Non-mit. Resp
ATP Production
Satellite Cell- Differentiation
D
WT
WT+PA
CD36KO
CD36KO+PA
E

Figure 7

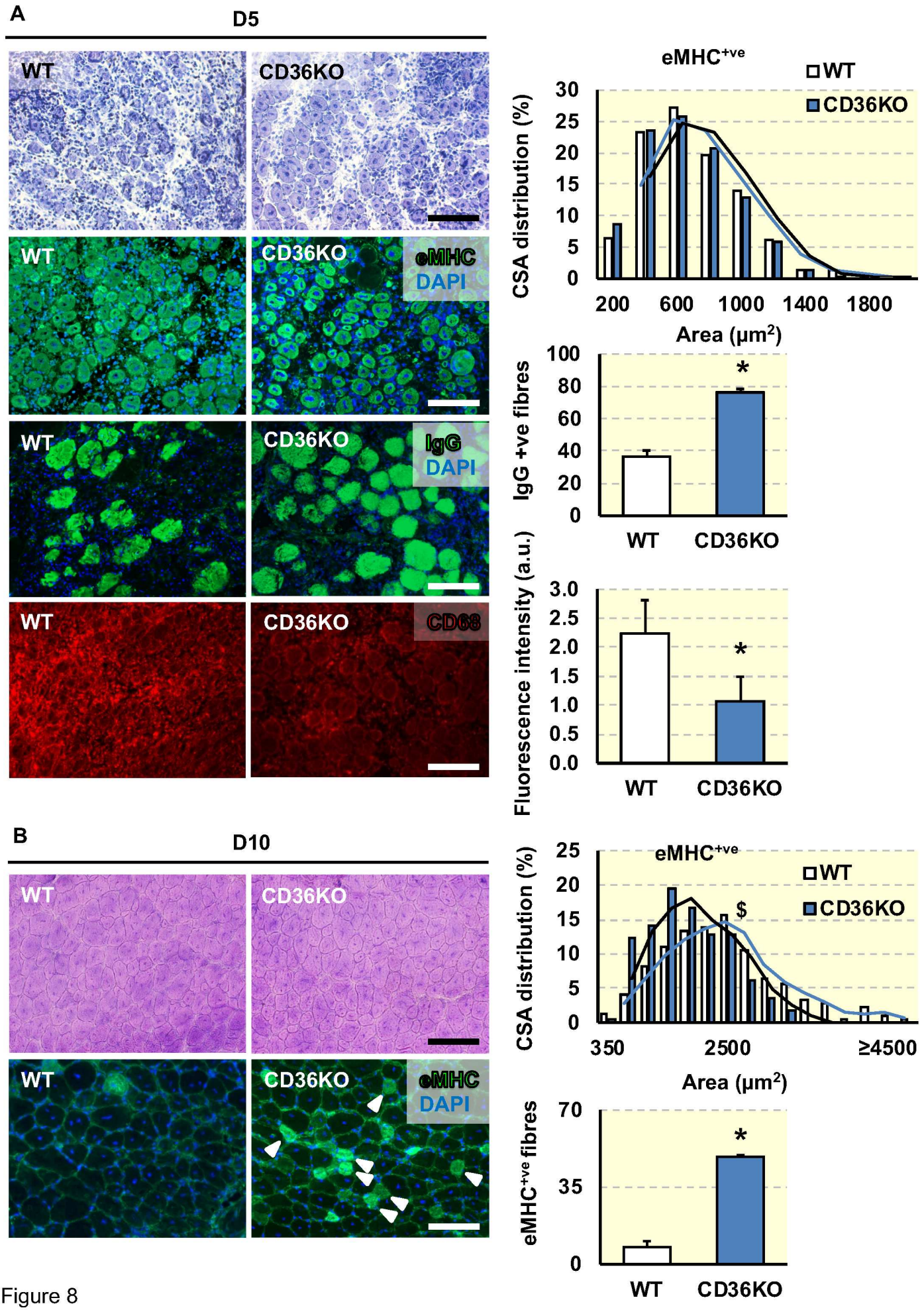
A
D5
WT
CD36KO
eMHC
DAPI
IgG
CD68
eMHC+ve
WT
CD36KO
CSA distribution (%)
Area (μm²)
IgG +ve fibres
Fluorescence intensity (a.u.)
B
D10
$
eMHC+ve fibres

Figure 8

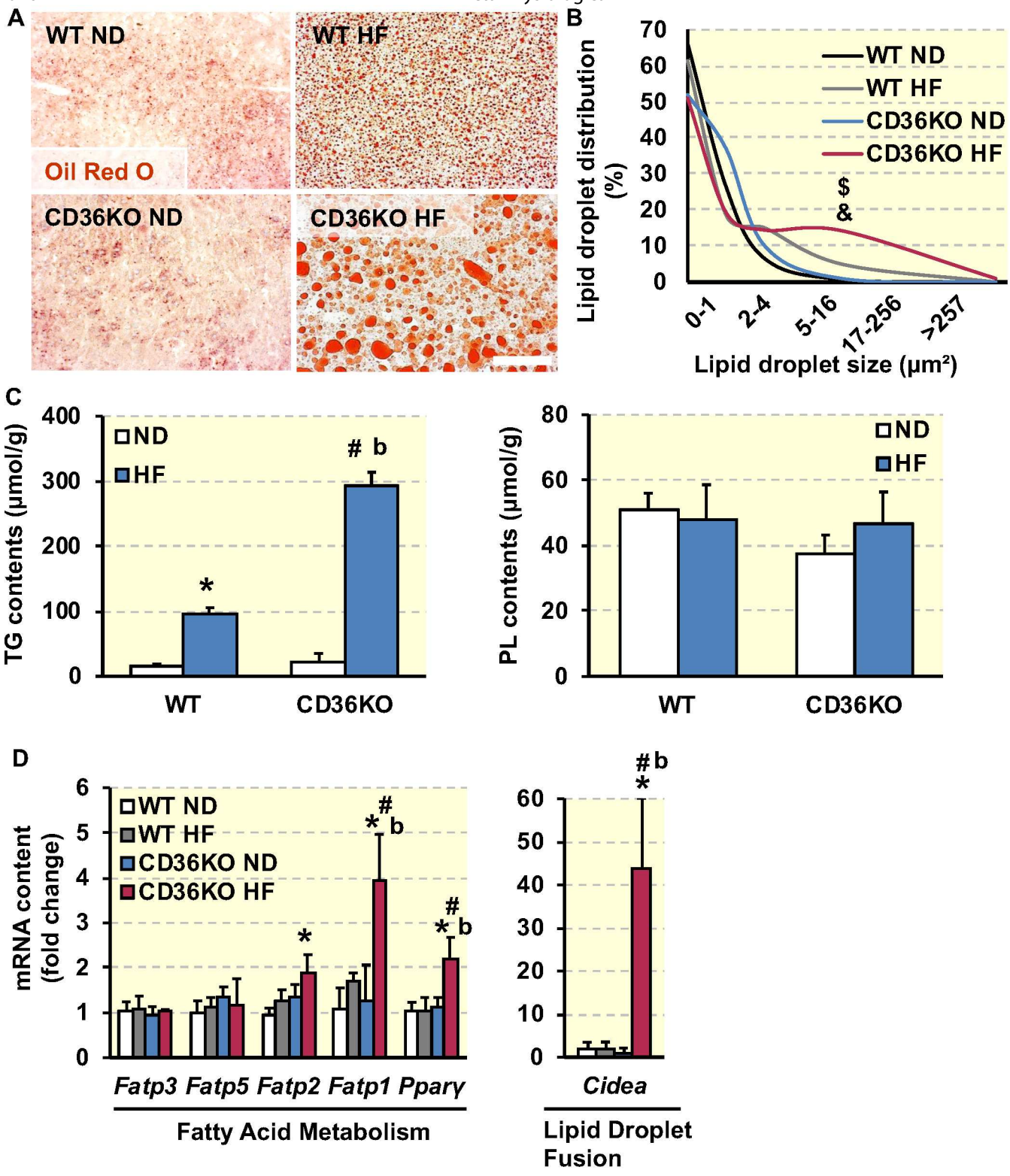
A
WT ND
WT HF
Oil Red O
CD36KO ND
CD36KO HF
B
Lipid droplet distribution (%)
WT ND
WT HF
CD36KO ND
CD36KO HF
$
&
0-1
2-4
5-16
17-256
>257
Lipid droplet size (μm²)
C
TG contents (μmol/g)
ND
HF
*
b
WT
CD36KO
PL contents (μmol/g)
ND
HF
WT
CD36KO
D
mRNA content (fold change)
WT ND
WT HF
CD36KO ND
CD36KO HF
*
*#b
*#b
Fatp3 Fatp5 Fatp2 Fatp1 Ppary
Fatty Acid Metabolism
#b
*
Cidea
Lipid Droplet Fusion

Figure 9

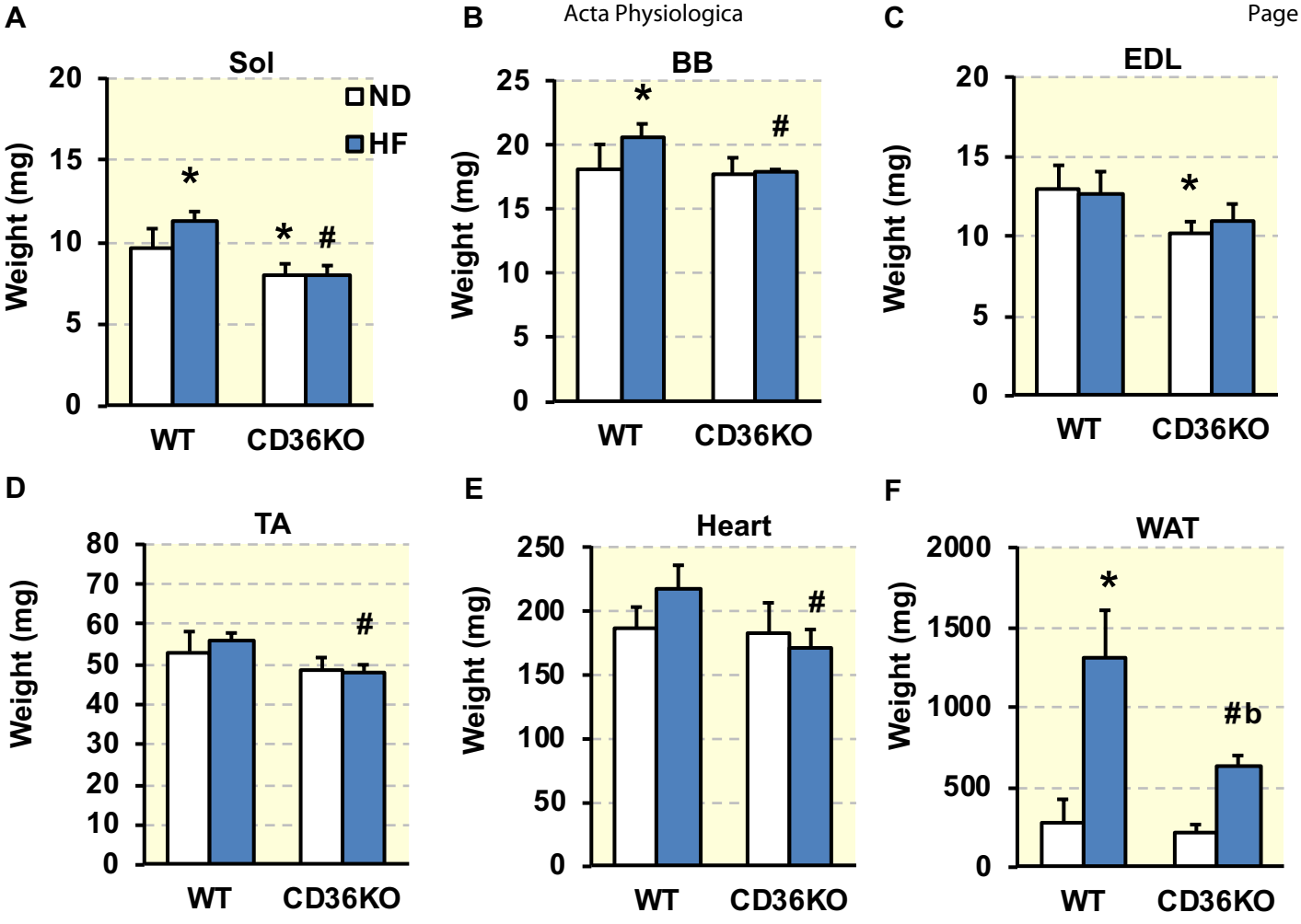
A
Sol
ND
HF
Weight (mg)
20
15
10
5
0
*
* #
WT
CD36KO
B
BB
Weight (mg)
25
20
15
10
5
0
*
#
WT
CD36KO
C
EDL
Weight (mg)
20
15
10
5
0
*
WT
CD36KO
D
TA
Weight (mg)
80
70
60
50
40
30
20
10
0
#
WT
CD36KO
E
Heart
Weight (mg)
250
200
150
100
50
0
#
WT
CD36KO
F
WAT
Weight (mg)
2000
1500
1000
500
0
*
#b
WT
CD36KO

Suppl. Fig. 1

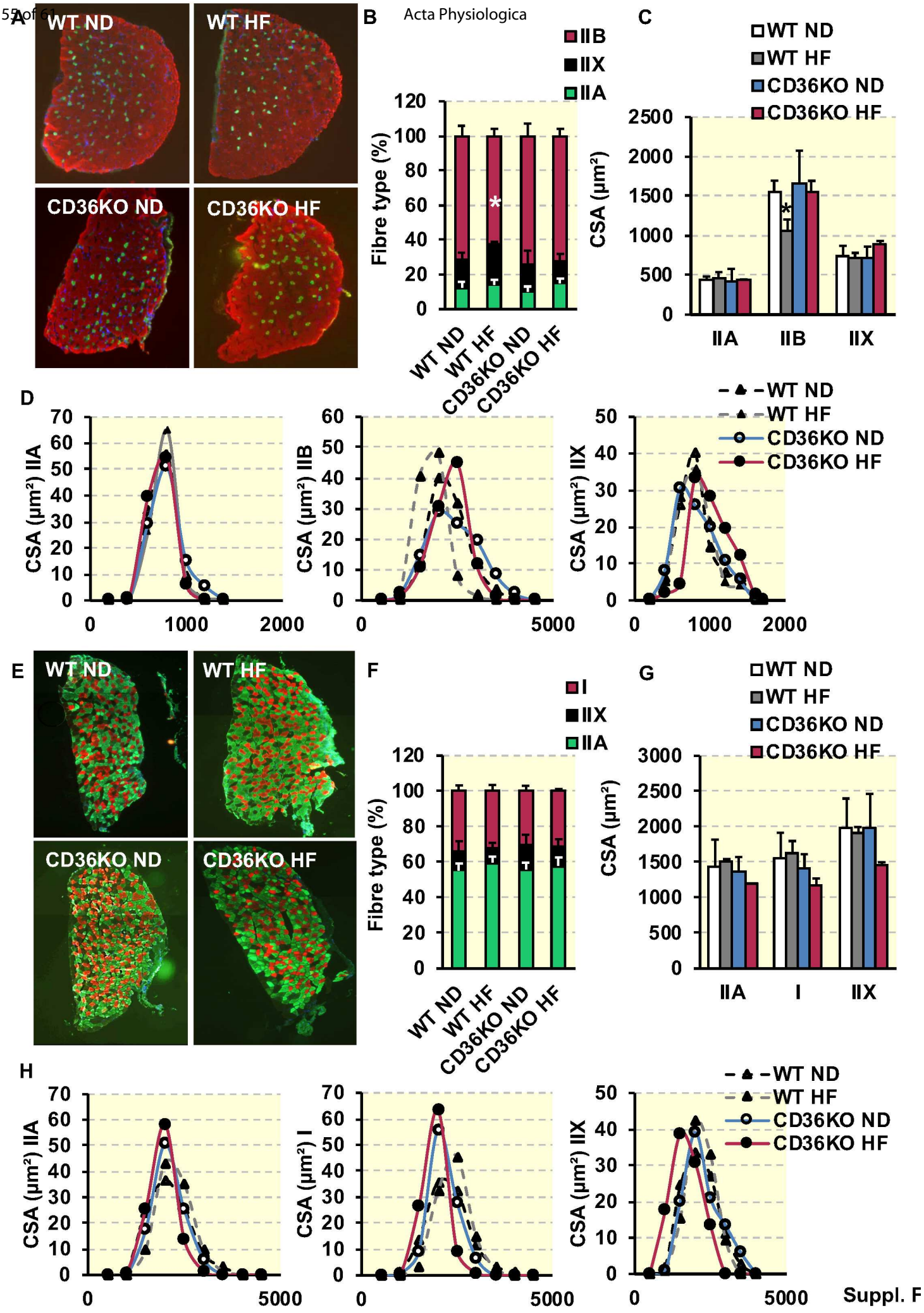
A
WT ND
WT HF
CD36KO ND
CD36KO HF
B
IIB
IIX
IIA
Fibre type (%)
WT ND
WT HF
CD36KO ND
CD36KO HF
C
WT ND
WT HF
CD36KO ND
CD36KO HF
CSA (µm²)
IIA
IIB
IIX
D
CSA (µm²) IIA
CSA (µm²) IIB
CSA (µm²) IIX
WT ND
WT HF
CD36KO ND
CD36KO HF
E
WT ND
WT HF
CD36KO ND
CD36KO HF
F
I
IIX
IIA
Fibre type (%)
WT ND
WT HF
CD36KO ND
CD36KO HF
G
WT ND
WT HF
CD36KO ND
CD36KO HF
CSA (µm²)
IIA
I
IIX
H
CSA (µm²) IIA
CSA (µm²) I
CSA (µm²) IIX
WT ND
WT HF
CD36KO ND
CD36KO HF

Suppl. F

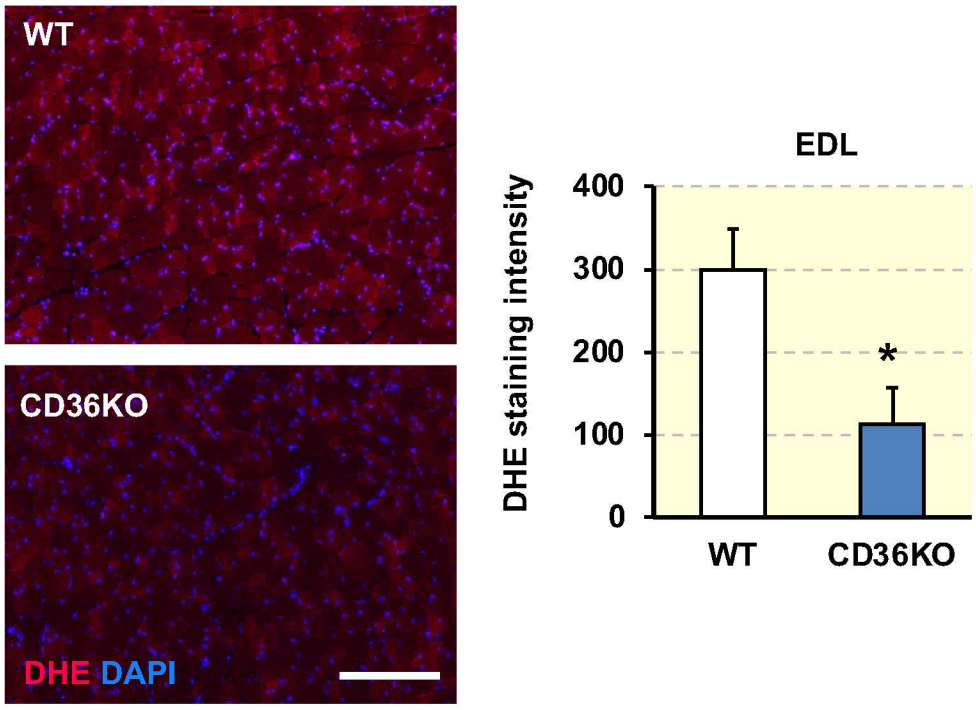
WT
CD36KO
DHE DAPI
EDL
DHE staining intensity
400
300
200
100
0
*
WT
CD36KO

Suppl. Fig. 3

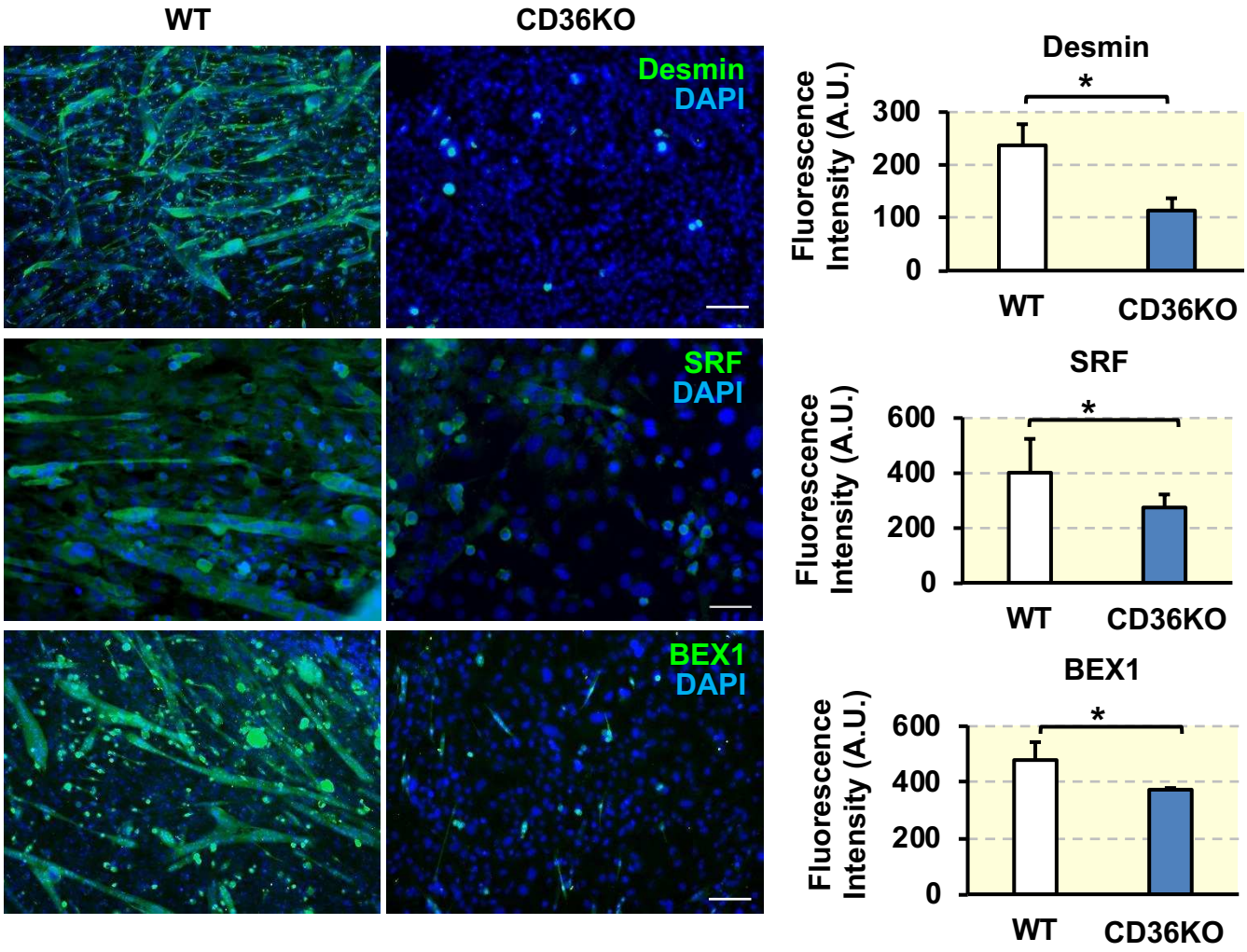
WT
CD36KO
Desmin
DAPI
SRF
DAPI
BEX1
DAPI
Desmin
Fluorescence Intensity (A.U.)
300
200
100
0
*
WT
CD36KO
SRF
Fluorescence Intensity (A.U.)
600
400
200
0
*
WT
CD36KO
BEX1
Fluorescence Intensity (A.U.)
600
400
200
0
*
WT
CD36KO

Suppl. Fig. 4

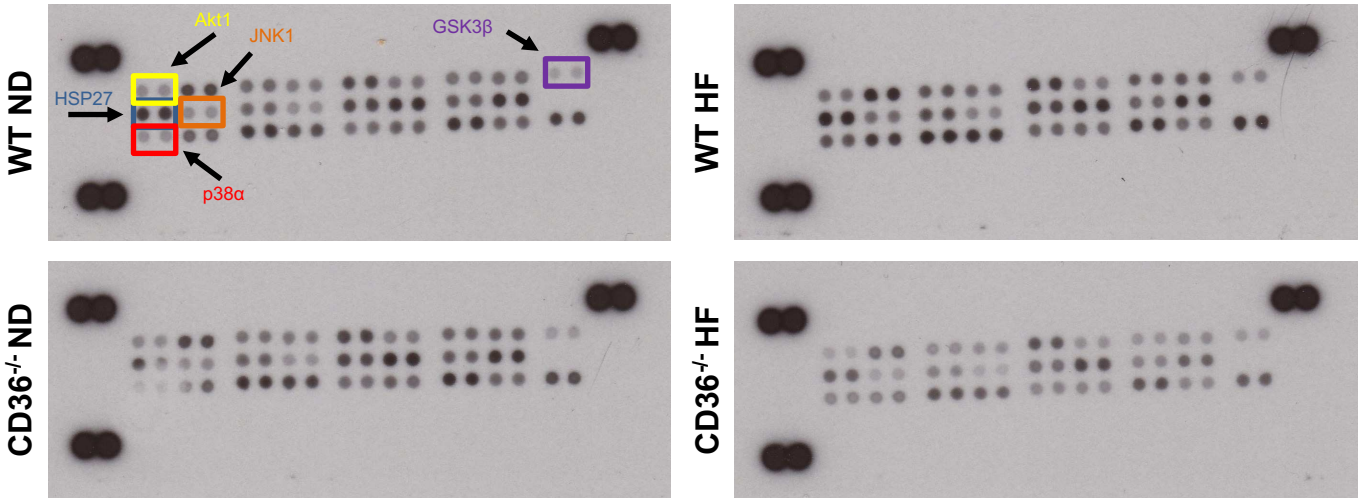

MAPKs	Fold Changes			
	vs. WT ND			vs. CD36$^{-/-}$ ND
	CD36$^{-/-}$ ND	WT HF	CD36$^{-/-}$ HF	CD36$^{-/-}$ HF
Akt1^{S473}	1.00	**1.52**	**0.53**	**0.52**
Akt2^{S474}	0.98	1.21	**0.67**	**0.68**
Akt3^{S472}	0.81	1.15	**0.53**	**0.65**
Akt Pan^{S473,S474,S472}	0.97	1.24	**0.62**	**0.64**
CREB^{S133}	1.07	1.15	**0.84**	**0.79**
ERK1$^{T202/Y204}$	0.93	0.90	**0.56**	**0.60**
ERK2$^{T185/Y187}$	1.07	1.12	**0.46**	**0.43**
GSK3α/β$^{S21/S9}$	1.01	1.10	**0.55**	**0.55**
GSK3β^{S9}	1.08	**1.65**	1.01	0.94
HSP27$^{S78/S82}$	**0.54**	1.19	**0.67**	1.23
JNK1$^{T183/Y185}$	0.95	**1.63**	**0.63**	**0.66**
JNK2$^{T183/Y185}$	1.02	1.28	**0.60**	**0.59**
JNK3$^{T221/Y223}$	0.90	1.17	**0.47**	**0.53**
JNK pan$^{T183/Y185,T221/Y223}$	1.01	1.05	**0.68**	**0.67**
MKK3$^{S218/T222}$	1.08	1.03	**0.81**	**0.75**
MKK6$^{S207/T211}$	0.93	0.87	**0.54**	**0.58**
MSK2^{S360}	0.95	0.91	**0.56**	**0.59**
p38α$^{T180/Y182}$	**0.19**	**2.29**	1.18	**6.19**
p38β$^{T180/Y182}$	**0.69**	1.38	**0.65**	0.94
p38δ$^{T180/Y182}$	0.98	1.13	**0.74**	**0.76**
p38γ$^{T183/Y185}$	1.11	1.29	**0.77**	**0.69**
p53^{S46}	1.05	1.16	**0.70**	**0.66**
p70S6K$^{T421/S424}$	0.98	0.94	**0.56**	**0.57**
RSK1^{S380}	1.00	0.95	**0.71**	**0.71**
RSK2^{S386}	0.92	0.91	**0.54**	**0.58**
TOR	0.96	1.15	**0.75**	**0.79**

Suppl. Fig. 5

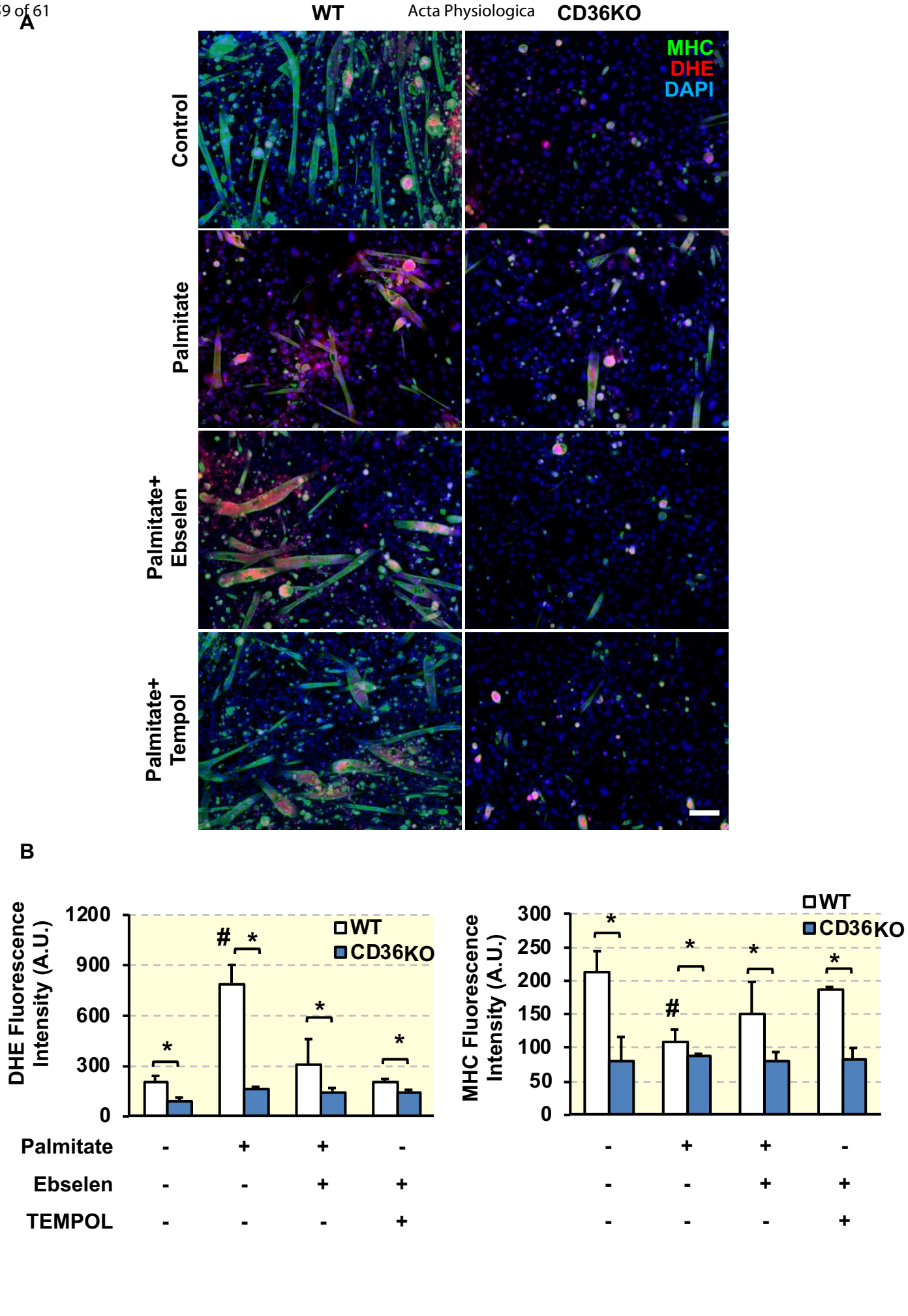
A
WT
CD36KO
MHC
DHE
DAPI
Control
Palmitate
Palmitate+ Ebselen
Palmitate+ Tempol
B
DHE Fluorescence Intensity (A.U.)
1200
900
600
300
0
WT
CD36KO
Palmitate - + + -
Ebselen - - + +
TEMPOL - - - +
MHC Fluorescence Intensity (A.U.)
300
250
200
150
100
50
0

Suppl. Fig. 6

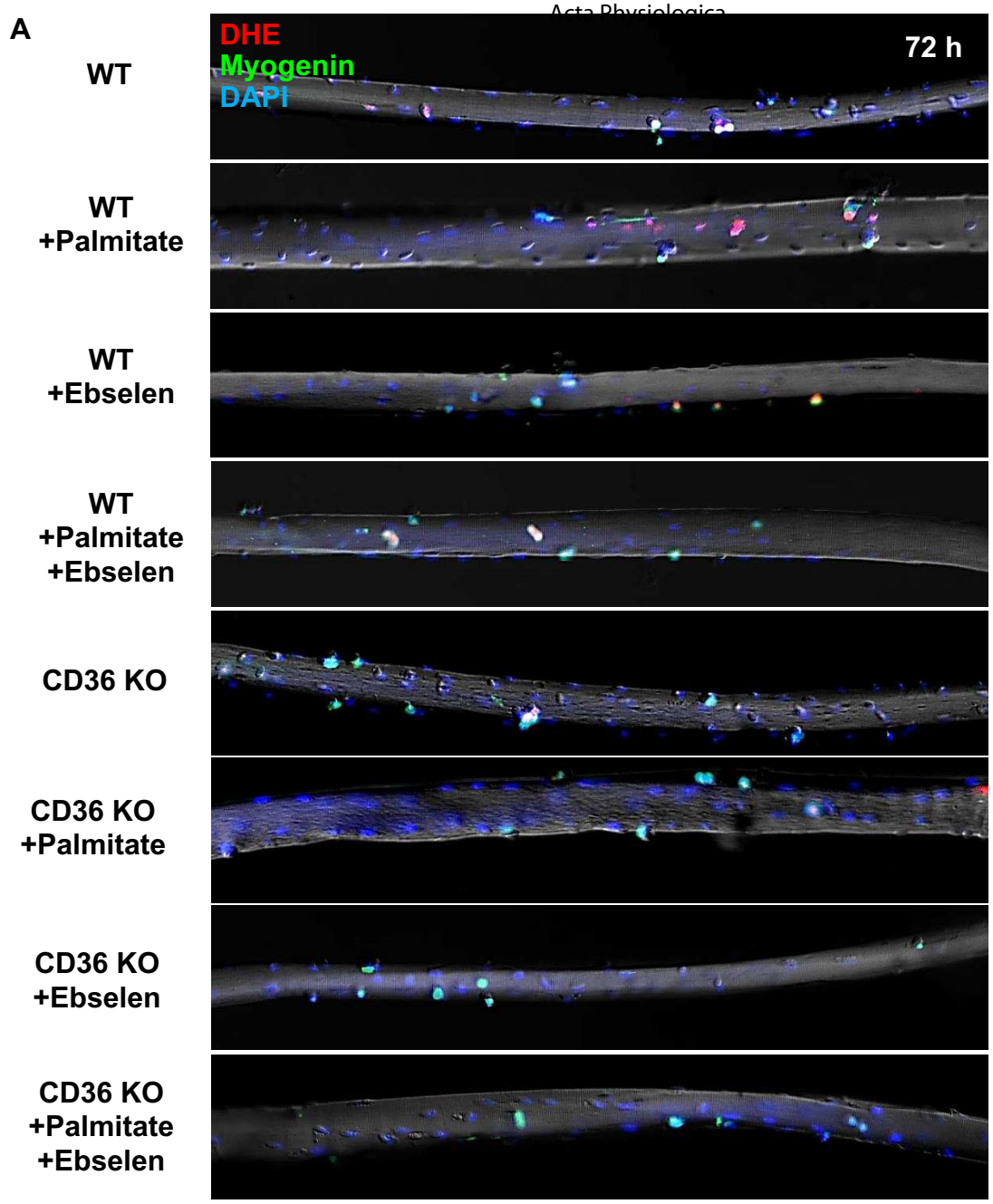
A
DHE
Myogenin
DAPI
72 h
WT
WT +Palmitate
WT +Ebselen
WT +Palmitate +Ebselen
CD36 KO
CD36 KO +Palmitate
CD36 KO +Ebselen
CD36 KO +Palmitate +Ebselen

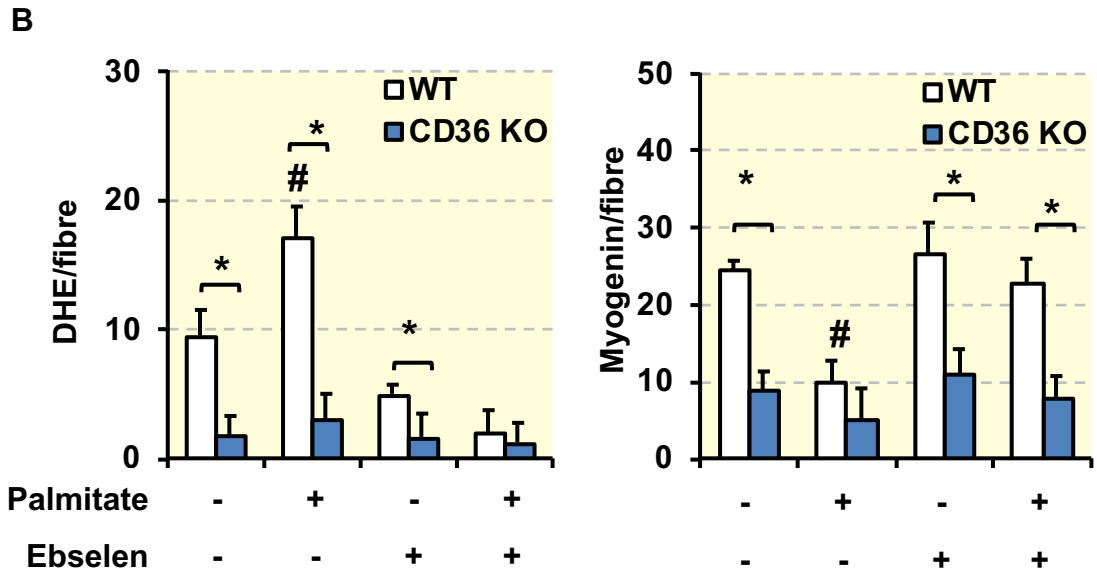
B
DHE/fibre
Myogenin/fibre
WT
CD36 KO
Palmitate
Ebselen
0
10
20
30
40
50
*
#

Suppl. Fig. 7

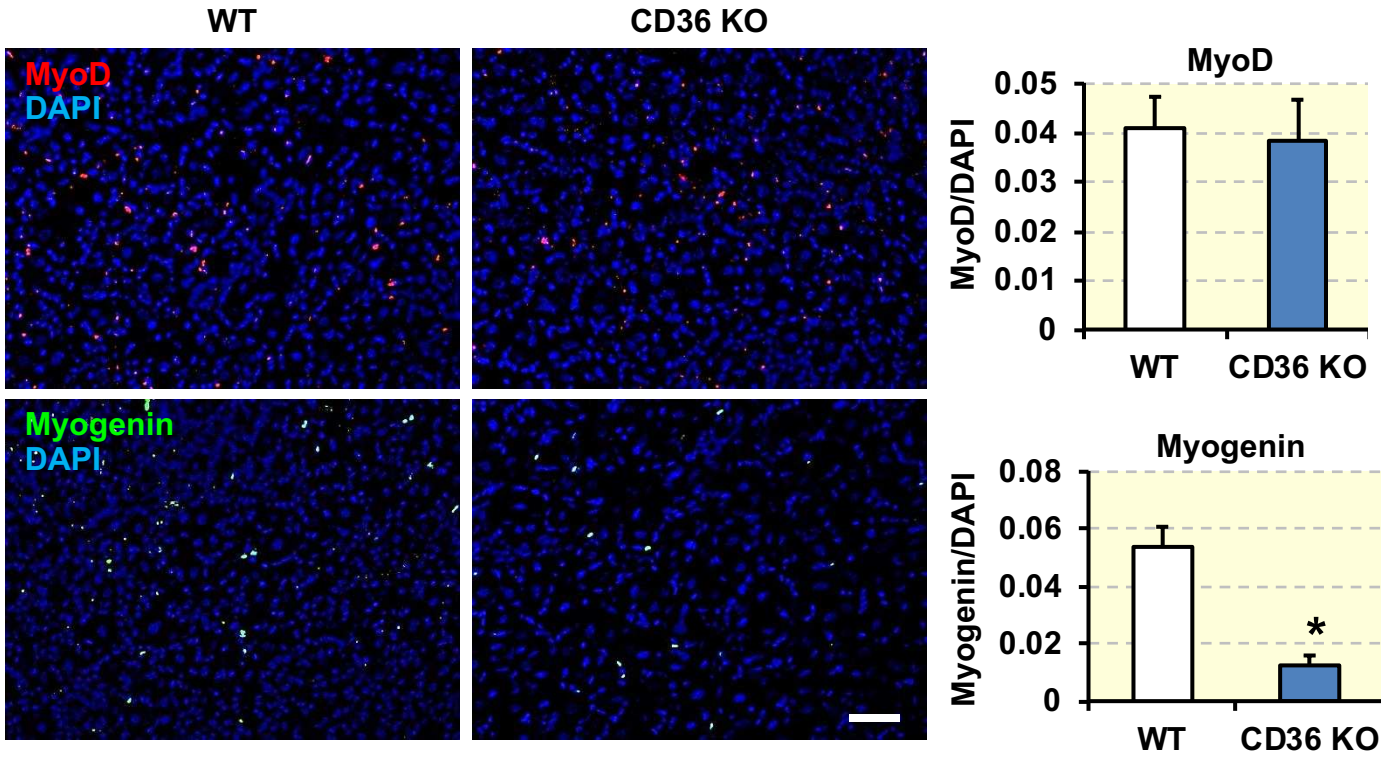
WT
CD36 KO
MyoD
DAPI
Myogenin
DAPI
MyoD
MyoD/DAPI
0.05
0.04
0.03
0.02
0.01
0
WT
CD36 KO
Myogenin
Myogenin/DAPI
0.08
0.06
0.04
0.02
0
*
WT
CD36 KO

Suppl. Fig. 8